

Review

Open Access



Asymmetrically coordinated single-atom catalysts: from synthetic strategy to structure-activity relationship

Tian Xia^{1,2,#}, Xiaofeng Wang^{2,3,#}, Jiawei Wan^{2,3,*}, Jian Qi^{2,3}, Dan Wang^{2,4,*}, Ranbo Yu^{1,4,*}

¹School of Metallurgical and Ecological Engineering, University of Science and Technology Beijing, Beijing 100083, China.

²State Key Laboratory of Biopharmaceutical Preparation and Delivery, Institute of Process Engineering, Chinese Academy of Sciences, Beijing 100190, China.

³University of Chinese Academy of Sciences, Beijing 101408, China.

⁴College of Chemistry and Environment Engineering, Shenzhen University, Shenzhen 518060, Guangdong, China.

#Authors contributed equally.

*Correspondence to: Prof. Jiawei Wan, State Key Laboratory of Biopharmaceutical Preparation and Delivery, Institute of Process Engineering, Chinese Academy of Sciences, Beijing 100190, China. E-mail: jwwan@ipe.ac.cn; Prof. Dan Wang, Prof. Ranbo Yu, College of Chemistry and Environment Engineering, Shenzhen University, Shenzhen 518060, Guangdong, China. E-mail: danwang@szu.edu.cn; ranboyu@ustb.edu.cn

How to cite this article: Xia, T.; Wang, X.; Wan, J.; Qi, J.; Wang, D.; Yu, R. Asymmetrically coordinated single-atom catalysts: from synthetic strategy to structure-activity relationship. *Chem. Synth.* 2025, 5, 74. <https://dx.doi.org/10.20517/cs.2025.08>

Received: 15 Jan 2025 **First Decision:** 9 May 2025 **Revised:** 12 Jun 2025 **Accepted:** 30 Jun 2025 **Published:** 12 Sep 2025

Academic Editor: Jin Xie **Copy Editor:** Pei-Yun Wang **Production Editor:** Pei-Yun Wang

Abstract

Asymmetric coordination structures in single-atom catalysts (SACs) represent a frontier in electrocatalysis, offering tunable electronic environments and enhanced catalytic performance beyond traditional symmetric M–N₄ motifs. This review first categorizes asymmetric SACs into four structural families: (1) single-metal asymmetric coordination, achieved by heteroatom substitution or axial ligand incorporation; (2) non-contact multi-metal sites, where adjacent but unbonded metal atoms synergize electronically; (3) directly bimetallic-bonded asymmetric coordination structures; and (4) bridged multi-metal constructs connected via non-metal linkers (e.g., O, N, S). Key synthetic strategies, including metal–organic framework confinement, defect engineering, dual-solvent loading, and macrocyclic precursor mediation, are examined in detail. Then we summarize applications in oxygen reduction reaction and CO₂ reduction reaction catalysis, and highlight how asymmetric coordination tunes intermediate adsorption energies, breaks scaling relations, and enables tandem catalysis to improve activity, selectivity, and stability. Advanced characterization techniques - aberration-corrected scanning transmission electron microscopy with electron energy loss spectroscopy, synchrotron X-ray absorption spectroscopy, and time-of-flight secondary ion mass spectrometry - are discussed for their roles in resolving atomic dispersion, coordination environment,



© The Author(s) 2025. **Open Access** This article is licensed under a Creative Commons Attribution 4.0 International License (<https://creativecommons.org/licenses/by/4.0/>), which permits unrestricted use, sharing, adaptation, distribution and reproduction in any medium or format, for any purpose, even commercially, as long as you give appropriate credit to the original author(s) and the source, provide a link to the Creative Commons license, and indicate if changes were made.



oxidation states, and dynamic evolution under operando conditions. Finally, challenges and future directions are outlined, including precise low-temperature assembly of heteronuclear sites, scalability, long-term stability under harsh reaction conditions, selective pathway control, and the integration of operando analyses with theoretical modeling to guide rational catalyst design.

Keywords: Single-atom catalysts, asymmetric coordination, electrocatalysis, oxygen reduction reaction, CO₂ reduction reaction

INTRODUCTION

Fossil fuel extraction and utilization have triggered severe environmental problems, giving rise to an urgent global energy and environmental crisis. Efficient and clean energy storage and conversion technologies are essential for sustainable development, and, in the context of carbon peaking and carbon neutrality, mitigating CO₂ emissions and promoting its valorization have emerged as critical objectives^[1,2]. Electrochemical conversion of hydrogen energy represents a viable strategy for mitigating carbon dioxide emissions. Among the key reactions in hydrogen energy conversion, the oxygen reduction reaction (ORR) decisively influences the overall efficiency of hydrogen utilization^[3-6]. In parallel, the electrochemical carbon dioxide reduction reaction (CO₂RR), which converts CO₂ into higher-value carbon-based products, such as CO, CH₄, and HCOOH, holds tremendous promise for facilitating CO₂ transformation^[7-10]. It is noteworthy that nearly all energy conversion and storage technologies depend on high-efficiency catalysts^[11-13]. Therefore, developing high-performance catalysts is essential for meeting sustainable development objectives. Although noble-metal catalysts exhibit superior intrinsic activity, their high cost and scarcity substantially impede large-scale practical deployment. Accordingly, designing catalysts that combine affordability with robust stability has become a critical priority in catalytic technology advancement^[14].

Single-atom catalysts (SACs) have garnered extensive attention owing to their remarkable atomic utilization efficiency and distinctive structural features^[15-17]. SACs consist of isolated metal atoms anchored on supports, offering atomically precise active centers, maximal metal utilization, and high structural tunability^[18-20]. These features endow SACs with exceptional catalytic activity and selectivity. As a rapidly evolving class of supported metal catalysts, these catalysts are regarded as among the most promising materials for electrochemical applications^[21-24].

In recent years, SACs with asymmetric coordination structures have gained considerable attention because of their unique properties and notable advancements^[8]. Building on symmetrically coordinated SACs, researchers have successfully synthesized a range of SACs with asymmetric coordination structures by fine-tuning the types and ratios of metal precursors, coordinating atoms, and supports. These catalysts often exhibit outstanding catalytic performance and stability^[25]. As an extension of symmetrically coordinated SACs, catalysts with asymmetric coordination mark a pivotal advancement. However, significant obstacles persist in synthesizing and characterizing atomic-site catalysts with asymmetric coordination structures. This review initially classifies asymmetrically coordinated SACs into two main categories: single-metal asymmetric coordination structures and multi-metal asymmetric coordination structures. Subsequently, the primary synthetic approaches for constructing asymmetrically coordinated SACs are detailed, and a summary of their ORR and CO₂RR applications is provided. Finally, the key characterization techniques for these materials are succinctly discussed, and an outlook on the future development of asymmetric coordination structures is provided.

CONSTRUCTION AND STRUCTURAL CHARACTERISTICS OF ASYMMETRIC COORDINATION STRUCTURES

The M_1-N_4 configuration (where M is a metal atom and N is nitrogen) is a common active-center structure in single-atom electrocatalysts^[26-29]. However, due to the relatively high electronegativity of the coordinated nitrogen atoms in the planar M_1-N_4 structure, the metal atom at the active center can bind reaction intermediates either too strongly or too weakly, resulting in sluggish catalytic kinetics and consequently hindering further improvements in electrocatalytic performance^[30-33]. To address this issue, researchers have modulated the local coordination environment of the central metal atom by introducing heteroatoms (e.g., P, S, Cl^[34-37]) to partially substitute for the coordinated nitrogen atoms, thereby constructing SACs with asymmetric coordination structures. This asymmetric coordination structure significantly modifies the electronic structure of the active center, effectively enhancing its catalytic activity during the reaction^[38,39].

Catalysts with Multi-metal asymmetric coordination structures are atomic-level catalysts formed by introducing one or more metal atoms into a single-metal asymmetric coordination structure, thereby creating multiple metal sites or active centers with asymmetric coordination structures. These structures can be regarded as an extension of single-atom sites^[40,41]. Catalysts with multi-metal asymmetric coordination architectures, building upon the advantages of single-atom (SA) catalysts, further optimize the adsorption states of reactants and intermediates, mitigate excessively strong or weak adsorption energies, disrupt linear scaling relationships among adsorbates, and enhance metal-atom loading^[42-44]. Furthermore, the introduction of heterogeneous metals in multi-metal asymmetric coordination structures can effectively modify the electronic structure of the catalysts^[41,45]. This modification involves regulating the charge state of active sites, altering electronic delocalization and orbital energy levels, and adjusting the d-orbital states of metal centers, which collectively optimize the electronic spin configuration. As a result, these changes influence the bonding and antibonding interactions with reactants, leading to improved adsorption and desorption processes^[46,47]. In addition, for various reactions, synergistic interactions among the multiple metals can trigger *in situ* structural evolution under reaction conditions, thereby forming more favorable structural configurations. Consequently, catalysts with multi-metal asymmetric coordination structures exhibit excellent catalytic performance and significant potential in electrocatalysis^[48-53].

In this chapter, we classify atomic-site catalysts with asymmetric coordination structures into two major categories: single-atom asymmetric structures and multi-metal asymmetric coordination structures. Based on the morphological characteristics of multi-metal asymmetric coordination structures, these catalysts can be further divided into non-contact multi-metal, directly bimetallic-bonded, and bridged multi-metal asymmetric coordination structures. The main strategies for synthesizing these distinct types of catalysts and their corresponding structural features are discussed individually.

Single-metal asymmetric coordination structures

Single-metal asymmetric coordination structures are constructed on the basis of the conventional $M-N_4$ coordination motif by introducing additional heteroatoms either within the $M-N_4$ equatorial plane or along the axial direction of the active center, and by tuning the coordination number of the active site. Such modifications can modulate the charge distribution at the catalytic site, the d-band center, and the adsorption state, thereby enhancing catalytic activity. Employing this strategy to improve the overall performance of SACs has emerged as a highly effective and broadly applicable approach.

Based on this, Wan *et al.* encapsulated triphenylphosphine (PPh_3) within a Zn/Co bimetallic metal-organic framework (MOF) cage and pyrolyzed it under argon at 950 °C to obtain a Co-SA/P catalyst bearing $Co_1-P_1N_3$ active sites [Figure 1A]^[54]. During the pyrolysis process, the metal Zn in the precursor evaporates

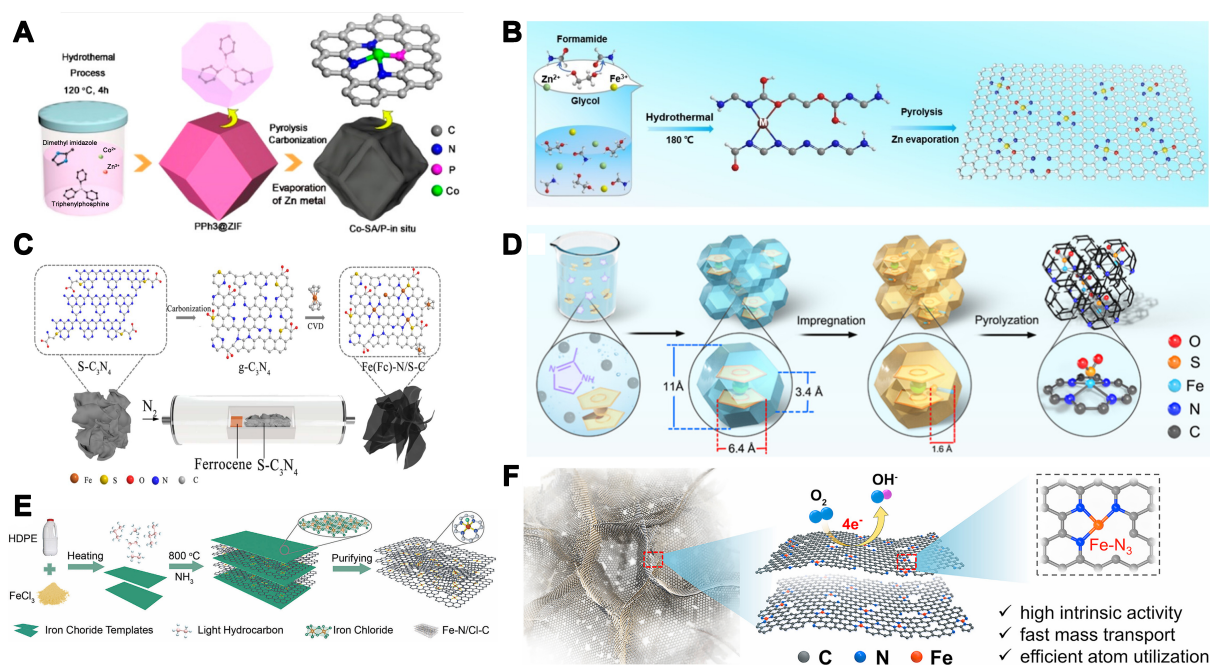


Figure 1. (A) Synthesis and morphological characterizations of Co-SA/P-*in situ* [54]. Copyright 2020, American Chemical Society; (B) Schematic diagram of synthesized Fe-N/O-C [55]. Copyright 2024, Wiley-VCH; (C) Typical CVD procedures to synthesize the Fe(Fc)-N/S-C catalyst [56]. Copyright 2021, American Chemical Society; (D) Schematic illustration of the synthesis of the Fe₁-N₄SO₂/NC catalyst [57]. Copyright 2025, American Chemical Society; (E) Schematic illustration and characterization of the Fe-N/Cl-C catalyst synthesized from HDPE [58]. Copyright 2025, Wiley-VCH; (F) Schematic diagram of the synthesis route for SACs-Mn-1000@g-C₃N₄ [60]. Copyright 2021, Cell Press. SA: Single-atom; CVD: chemical vapor deposition; HDPE: high-density polyethylene; SACs: single-atom catalysts.

and forms isolated Co atomic sites on the carbon support. ZIF-67 was used as the precursor to encapsulate PPh₃, and the Co₁-P₁N₃ site-containing Co particles/Co₁-P₁N₃ composite catalyst was obtained by pyrolysis at 900 °C under a nitrogen atmosphere. The approach of generating single atoms through vacancies induced by Zn evaporation at elevated temperatures is widely applicable. Li *et al.* synthesized an Fe-N/O-C catalyst composed of Fe-N₃O and adjacent defects [55]. Formamide, as both a reactant and solvent, serves as a nitrogen and carbon source. Fe salts, Zn salts, and ethylene glycol were mixed and subjected to hydrothermal reaction at 180 °C to obtain a single-atom precursor (Fe/Zn-N/O-C) with metal and N, O coordination structures, which was then pyrolyzed to evaporate Zn atoms and obtain the Fe-N/O-C catalyst. The authors pointed out that formamide molecules could undergo condensation via the Schiff base reaction and be used to chelate metal cations, thereby anchoring metal ions to form single atoms [Figure 1B]. Moreover, employing C₃N₄ as a support for constructing these catalysts represents an effective strategy. Li *et al.* employed chemical vapor deposition to fabricate an Fe-N/S-C SAC on S-doped C₃N₄ [56]. A melamine/cysteine precursor was carbonized at 600 °C under N₂ to produce N,S-doped C₃N₄ nanosheets rich in carbon defects and C-S-C motifs. Subsequent pyrolysis with ferrocene (20:1 mass ratio) at 900 °C under N₂ anchored Fe atoms at these defect sites, yielding stabilized Fe-N/S active sites and suppressing iron carbide formation [Figure 1C].

Furthermore, introducing axially coordinated non-metal atoms into the traditional M-N₄ structures, as well as adjusting the central metal's coordination number to form M-N_{4-x} structures, are both key approaches to constructing single-atom asymmetric coordination architectures. A brief overview of their synthesis methods is provided below.

In the preparation of catalysts with axial coordination, Qu *et al.* employed potassium thiocyanate (KSCN) as the sulfur-oxygen dopant, impregnated it onto a $\text{FeCp}_2\text{@ZIF-8}$ precursor via ultrasonication and stirring in methanol, and then pyrolyzed the dried composite under N_2 at 950 °C for 3 h to yield $\text{Fe}_1\text{-N}_4\text{SO}_2\text{/NC}$ featuring atomically dispersed $\text{Fe}_1\text{-N}_4\text{SO}_2$ coordination sites on a carbon matrix [Figure 1D]^[57]. In addition, Ren *et al.* impregnated high-density polyethylene (HDPE) with FeCl_3 , pyrolyzed under NH_3 at 800 °C for 3 h (5 °C·min⁻¹), then acid-etched in HCl to remove residual iron, yielding graphene-supported Fe-N/Cl-C with atomically dispersed FeN_4Cl sites [Figure 1E]^[58]. Besides, modulating the coordination number between active centers and nitrogen atoms offers an effective route to asymmetric coordination structures. Yan *et al.* precipitated a glycine- MgCl_2 complex, mixed it with Co(OAc)_2 , pyrolyzed under N_2 at 800 °C for 2 h, then HCl-etched to remove MgO/Co particles, yielding carbon-supported $\text{Co-N}_5\text{C}$ with atomically dispersed CoN_5 sites^[59]. In 2021, Liu *et al.* hydrothermally self-assembled graphene oxide nanoribbons with FeCl_3 into a 3D hydrogel, freeze-dried, then acid-leached and calcined to yield $\text{eFe-N}_3\text{/PCF}$ - a porous carbon framework with edge-hosted Fe-N_3 sites, offering high intrinsic activity, fast mass transport, and efficient atom utilization [Figure 1F]^[60]. Qin *et al.* mixed Mn-ZIF-8 with $\text{g-C}_3\text{N}_4$ in ethanol, then subjected the mixture to pyrolysis, acid leaching, and a brief reheating to yield $\text{SACs-Mn-1000@g-C}_3\text{N}_4$, a graphene-like, hierarchically porous framework bearing Mn-N_3 sites anchored at defect sites^[61].

Non-contact multi-metal asymmetric coordination structures

Non-contact coordination structures differ from randomly dispersed single-atom structures. In non-contact coordination structures, although the metal atoms do not directly contact each other, the spacing between them needs to be sufficiently small (< 15 Å). Two metal atoms with sufficiently small spacing can interact to achieve the desired catalytic performance. Therefore, non-contact multi-metal asymmetric coordination structures have attracted extensive attention from researchers.

As reported by Zhang *et al.*, a quasi-double-star $\text{Ni}_7\text{/Fe}_3\text{-N-C}$ catalyst was produced via one-pot solvothermal incorporation of Ni and Fe into Zn-IRMOF-3 , followed by Ar-atmosphere pyrolysis at 950 °C for 2 h, yielding a carbon-supported material with atomically dispersed adjacent Ni and Fe SA sites^[62]. Han *et al.* encapsulated Pt(acac)_2 and Fe(acac)_3 in ZIF-8 and obtained $\text{Fe-N}_4\text{/Pt-N}_4\text{@NC}$ by pyrolyzing the precursor^[63]. Density functional theory (DFT) calculations showed that adjacent Pt-N_4 sites can effectively modulate the 3d electronic orbitals of Fe-N_4 sites, resulting in enhanced catalytic performance [Figure 2A]. Building on this concept of adjacent-site electronic modulation, Zhao *et al.* developed a low-temperature pyrolysis of diethylenetriaminepentaacetic-acid bimetallic complexes to produce dynamically stable carbon dots with embedded bimetallic atomic sites (DMASs-CDs)^[64]. As shown in Figure 2B, more than twenty DMASs-CDs incorporating Fe, Co, Ni, Mn, Zn, Cu, and Mo pairings were prepared. Notably, NiMn-CDs exhibited superior intrinsic activity in the urea oxidation probe reaction. By adjusting DMAS combinations, this method enables precise, target-oriented design of catalysts for various electrochemical processes. Remarkably, non-noble transition metals such as Co, Cu and Ni also furnish exceptional catalytically active sites. As shown in Figure 2C, the bifunctional oxygen electrocatalyst (Cu-Co/NC), comprising copper-cobalt dual-atom sites with optimized geometric and electronic structures on a high-porosity nitrogen-doped carbon (NC) support, was prepared by Li *et al.*^[65]. Specifically, after introducing copper acetate into Zn-Co MOF , they coated it with a polymer rich in nitrogen sources and then pyrolyzed it in an inert atmosphere at high temperatures to obtain the target catalyst. Experimental and theoretical results showed that Cu and Co atoms exist as atom pairs on the carbon-nitrogen support. Both Cu and Co formed M-N_4 coordination structures, with Cu in a +1 oxidation state and Co in a +2 oxidation state. After loading Cu and Co, the electronic properties of N and C changed, with N predominantly existing in the form of metal-pyridinic N. Similarly, Wu *et al.* synthesized $\text{SOD-[Zn(mim)}_2\text{]} (\text{MAF-4/ZIF-8, Hmim} = 2\text{-methylimidazole})$ by modulating the Zn/Co/Ni feed ratios during MOF synthesis under vigorous stirring^[66]. Under an N_2 atmosphere, the MOF precursors were combined with NH_4Cl and pyrolyzed at 900 °C to yield carbonized

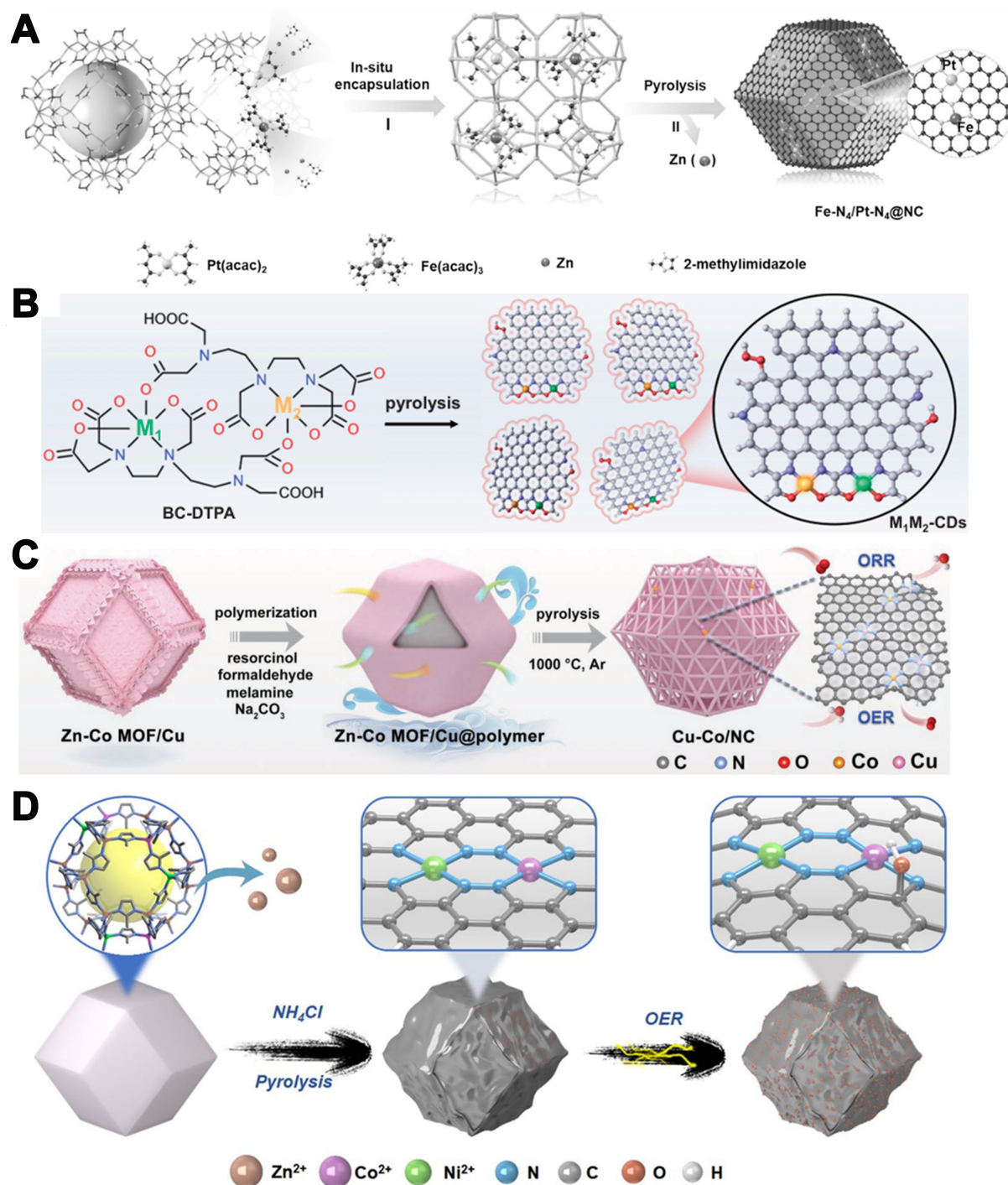


Figure 2. (A) Synthesis process of Fe-N₄/Pt-N₄@NC^[63]. Copyright 2021, Wiley-VCH; (B) Preparation and structure illustration of the “carbon islands” of DMASs-CDs (red: O atom, blue: N atom, gray: C atom, green: first metal atom, orange: second metal atom)^[64]. Copyright 2023, National Academy of Sciences; (C) Synthetic scheme of Cu-Co/NC^[65]. Copyright 2023, Wiley-VCH; (D) Schematic illustration of the synthetic processes and structures of AD-Co_xNi_{1-x} and O-AD-Co_xNi_{1-x}^[66]. Copyright 2023, Springer Nature. DMASs-CDs: Dynamically stable carbon dots with embedded bimetallic atomic sites.

samples. Inductively coupled plasma mass spectrometry (ICP-MS) quantification established the Co and Ni contents, and the products were designated AD-Co₁Ni₀, AD-Co_{0.72}Ni_{0.28}, AD-Co_{0.62}Ni_{0.38}, AD-Co_{0.48}Ni_{0.52}, AD-

$\text{Co}_{0.41}\text{Ni}_{0.59}$, AD- Co_0Ni_1 , and NC- $\text{Co}_{0.49}\text{Ni}_{0.51}$. Powder X-ray diffraction (PXRD) and high-resolution transmission electron microscopy (HRTEM) confirmed the absence of nanocrystals or nanoparticles/clusters. High-angle annular dark-field scanning transmission electron microscopy (HAADF-STEM) imaging revealed numerous bright spots on the carbon matrix, attributable to atomically dispersed Co and Ni atoms, many separated by distances less than 5.0 Å, suggesting the coexistence of multiple bimetallic site configurations [Figure 2D].

Directly bimetallic-bonded asymmetric coordination structures

Direct bimetallic-bonded asymmetric coordination structures refer to catalysts that contain two (or more) different or identical single-atom active sites, where these single-metal atoms are bonded to each other. Unlike metal alloys, these directly bonded metals can only be anchored into the substrate in single-atom form. Such interactions between metals often effectively optimize and regulate the electronic structure, coordination environment, electron spin configuration, and charge state of the active sites.

As shown in Figure 3A, Zhang *et al.* synthesized the Zn/Co/Ni imidazole zeolite framework (Zn/Co/Ni-ZIFs) precursor using cation exchange and cavity adsorption strategies, and finely tuned the structure of the target catalyst $\text{NiN}_3\text{CoN}_3\text{-NC}$ by adjusting the Zn content and pyrolysis temperature^[67]. Through aberration-corrected HAADF-STEM, 3D atomic overlap Gaussian fitting mapping, X-ray absorption fine structure (XAFS), and X-ray diffraction (XRD), they systematically confirmed the structural characteristics of $\text{NiN}_3\text{CoN}_3\text{-NC}$ (Ni-Co covalently coupled atom pair embedded in nitrogen-doped graphitized carbon). Moreover, Wang *et al.* synthesized C_2N supports featuring uniform N_6 cavities and edge N deficiencies by high-temperature pyrolysis of cyclohexanone and urea in the presence of MgCl_2 , providing optimal sites for metal anchoring^[68]. Fe and Sn precursors were subsequently introduced via wet impregnation followed by a second pyrolysis, yielding the FeSn- C_2N dual-atom catalyst with Fe and Sn atoms precisely anchored within the N_6 cavities, forming a robust structure. Energy band alignment between Sn p-orbitals and Fe d-orbitals enhanced p-d coupling and improved the catalyst's thermodynamic stability, underscoring its catalytic potential. XAFS characterization revealed that Fe in FeSn- C_2N exhibited a lower oxidation state than in Fe- C_2N , due to the polarization-charge effects induced by Sn incorporation. Fe K-edge FT-EXAFS confirmed Fe-Sn bonding at 2.22 Å, verifying the bimetallic coordination [Figure 3B]. Sn K-edge X-ray absorption near edge structure (XANES) indicated a reduced Sn oxidation state relative to Sn- C_2N , reflecting charge redistribution from strong Fe-Sn electronic interactions. In summary, the reduced oxidation states of Fe and Sn in FeSn- C_2N reflect the combined effect of Fe-Sn bimetallic electronic coupling and polarization charge redistribution.

Furthermore, Zhu *et al.* reported a Ni-Cu atomic pair catalyst (Ni/Cu-N-C) synthesized via a host-guest strategy [Figure 3C]^[69]. A Cu/1,10-phenanthroline complex (~9.5 Å) was encapsulated within a bimetallic NiZn zeolitic imidazolate framework (Ni-ZIF-8; cavity ~11.6 Å), ensuring isolated Cu sites in the ZIF micropores. Zn dilution and pore confinement favored the formation of Ni-Cu pairs over nanoparticles or single atoms. Characterization showed no metal nanoparticles and revealed a Ni-Cu interatomic distance of ~2.4 Å, indicating atomically dispersed metals with strong electronic coupling. To achieve highly active SACs, Pan *et al.*, guided by DFT and Monte Carlo (MC) simulation calculations, used a dual-solvent method to load Fe^{3+} and Ni^{2+} onto ZIF-8 as a template, followed by co-pyrolysis with sodium hypophosphite to obtain P-doped Fe-Ni dual-atom pair catalysts (Fe-Ni-N-P-C)^[70]. Both theoretical and experimental results successfully demonstrated the precise synthesis of the P-doped Fe-Ni dual-atom pair [Figure 3D].

As shown in Figure 3E, the facile atomic printing strategy to fabricate a series of $\text{M}_1\text{M}_2\text{-C}_2\text{N}$ materials was developed by Sun *et al.*^[71]. In a typical synthesis, a solid mixture of cyclohexanone and urea was heated at

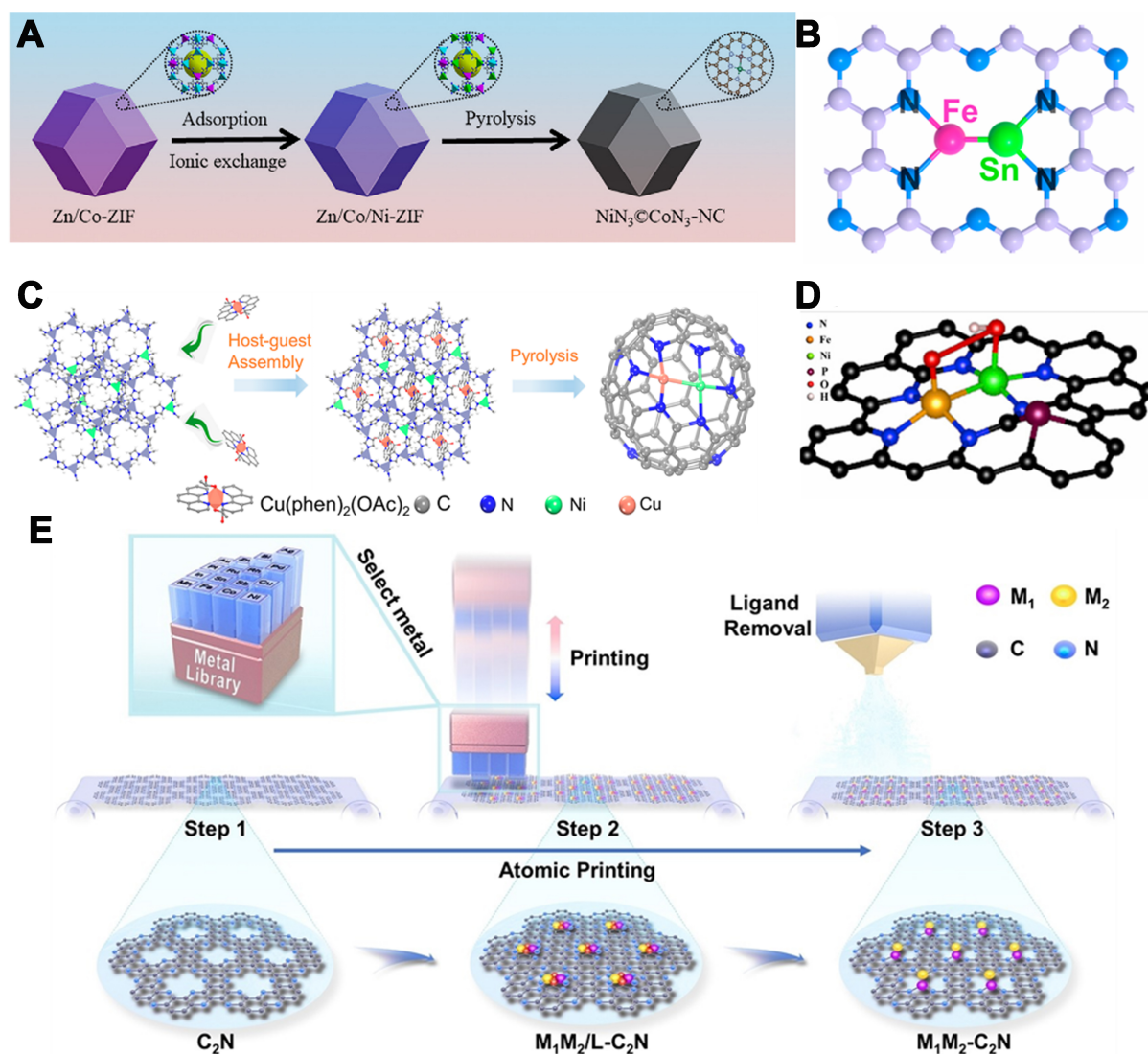


Figure 3. (A) Scheme illustration of the synthetic procedure of $\text{NiN}_3@\text{CoN}_3\text{-NC}$ ^[67]. Copyright 2023, Elsevier B.V; (B) The dimer structure of active FeSn dual atom sites derived from the EXAFS result^[68]. Copyright 2024, American Chemical Society; (C) Schematic illustration of the synthetic procedure of the diatomic Ni/Cu-N-C catalyst^[69]. Copyright 2022, American Chemical Society; (D) The geometric structure of Fe-Ni-N-P-C^[70]. Copyright 2021, Cell Press; (E) Schematic illustration of the synthesis of the C_2N ^[71]. Copyright 2024, Wiley-VCH. EXAFS: Extended X-ray absorption fine structure.

90 °C for 30 min to yield a crosslinked intermediate, which was then milled with anhydrous MgCl_2 in precise ratios. Calcination under N_2 at 900 °C for 2 h transformed the intermediate into C_2N , featuring a uniformly porous network rich in unsaturated nitrogen “clamps” that efficiently anchor metal dimers at vacancy sites via strong N coordination. During annealing, MgCl_2 and its crosslinked precursors generated HCl gas, facilitating the etching of metal nanoparticles and removal of organic ligands, thereby enabling the formation of two-dimensional $\text{M}_1\text{M}_2\text{-C}_2\text{N}$ structures. Furthermore Zhang *et al.* developed a defect-rich sulfur- and nitrogen-co-doped carbon support (SNC) to anchor Fe-Fe dual-atom sites (A- $\text{Fe}_2\text{S}_1\text{N}_3/\text{SNC}$) via a multilayer defect-trapping and coordination-locking strategy^[72]. Co-pyrolysis of 2-benzothiazolylthiol and melamine under inert atmosphere generated highly defective SNC nanosheets through radical polymerization and thermal decomposition, which then stabilized dual Fe atoms by sulfur coordination and vacancy trapping.

Bridged multi-metal asymmetric coordination structures

In Bridged multi-metal asymmetric coordination structures, there is no direct interaction between the metal atoms, but they are connected by non-metallic atoms (such as O, N, S). Under the influence of non-metallic atoms, the electronic density between bimetallic sites can be redistributed, which alters the charge state of the metals and enhances catalytic performance. Non-metallic bridging atoms with different electronegativities often result in completely different catalytic effects.

Based on this, Zhang *et al.* prepared planar-Fe-Co and stereo-Fe-Co dual-site catalysts (DSCs) through various electrochemical deposition methods^[73]. Experimental characterizations revealed the different spatial relationships between Fe single atoms and Co atoms in CoOOH substrates, confirming that the Fe and Co atoms in the catalysts exist in an Fe-O-Co form. Furthermore, Zhao *et al.* developed a dual-atom catalyst (DAC) synthesis approach at the simple-level stage by exploiting precise electrostatic control and engineered adjacent vacancies^[74]. As a proof of concept, they fabricated uniformly dispersed dual-iron sites bridged by two nitrogen atoms (Fe-N₂-Fe). Their method anchors a second Fe ion at pre-existing SAC sites using bridging nitrogen precursors; subsequent pyrolysis etches neighboring carbon atoms to form vacancies that trap the second ion [Figure 4A]. Similarly, Sun *et al.* noted that incorporating sulfur ligands into SACs typically requires high-temperature pyrolysis to convert solid sulfur into gaseous species for substrate etching, a process that usually yields only monometal-sulfur coordination at bimetallic sites, precluding sulfur-bridged architectures^[75]. To address this, they employed wool-derived keratin as a support to construct a dual-metal catalyst featuring novel Cu-S-Ni bridging sites (Cu-S-Ni/SNC). The abundant disulfide bonds in keratin serve as *in situ* sulfur donors, while the protein's partial long-range order provides defined anchoring sites for metal atoms. Additionally, X-ray absorption spectroscopy (XAS) elucidated the coordination geometry of the Cu-S-Ni sulfur-bridged bimetallic sites [Figure 4B].

Li *et al.* prepared a Co-N-Ni catalyst by co-grinding melamine, L-aspartic acid, Co(acac)₃, and Ni(acac)₂; adding ethanol/HCl and evaporating the solvent; then pyrolyzing under N₂ and cooling^[76]. Characterization confirmed that this polymerization-decomposition route precisely controls the N-bridged Co-Ni spacing [Figure 4C]. As shown in Figure 4D, Wang *et al.* developed an innovative metal ion recognition (MIR) strategy to address the challenges in the synthesis of dual-atom catalysts^[77]. This strategy involves the sequential adsorption of target cations and anions onto NC substrates to form precursors, enabling the synthesis of various DACs. Taking Fe₁Sn₁-DAC as an example, NC derived from ZIF-8 with rhombic dodecahedral morphology and negative surface charge was first prepared. Then, [Fe(bpy)₃]²⁺ and [SnCl₆]²⁻ were sequentially adsorbed to form a heterometallic bimetallic ion pair, followed by high-temperature pyrolysis to obtain Fe₁Sn₁-DAC. Multiple characterization techniques confirmed the successful synthesis of this catalyst, and theoretical calculations revealed the coordination structure of Fe and Sn. Additionally, other DACs such as Fe₁Co₁, Fe₁Ni₁, Fe₁Cu₁, Fe₁Mn₁, Co₁Ni₁, Co₁Cu₁, Co₂, and Cu₂ were also successfully synthesized, demonstrating the versatility of the strategy. Similarly, Zhang *et al.* introduced a macrocycle-mediated encapsulation-pyrolysis strategy for precise DAC synthesis^[78]. A Robson-type macrocycle embeds homo- and heteronuclear bimetallic centers within a planar ligand framework, and its confinement in porous carbon preserves the dual-atom motif during heat treatment. Employing this method, a Fe-Cu dual-atom site bridged by two oxygen atoms was constructed [Figure 4E].

APPLICATIONS OF ASYMMETRIC COORDINATION STRUCTURES IN ELECTROCHEMICAL REACTIONS

Single-metal asymmetric coordination structures

The coordination environment of the central metal in SACs has a crucial impact on catalytic performance. Studies have shown that incorporating the central atom with one or more coordination atoms of different

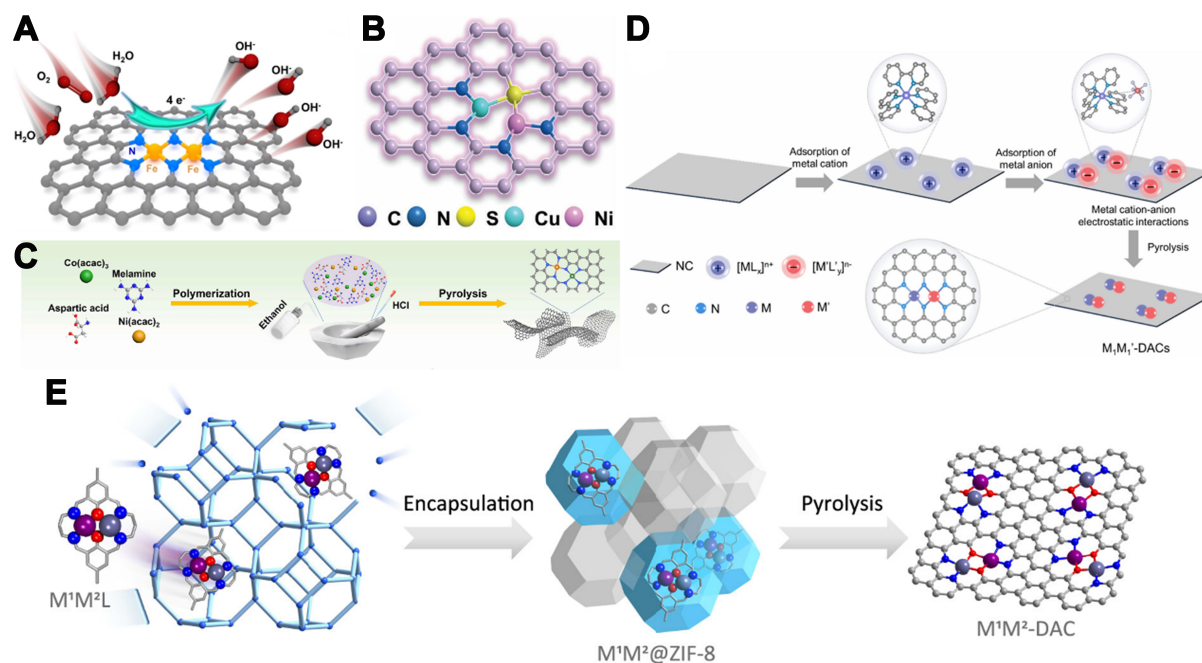


Figure 4. (A) Atomic structure model of Fe-N₂-Fe DAC^[74]. Copyright 2024, Wiley-VCH; (B) Atomic structure model of Cu-S-Ni/SNC^[75]. Copyright 2024, Wiley-VCH; (C) Schematic diagram of the polymerization-pyrolysis synthesis method of Co-N-Ni^[76]. Copyright 2023, American Chemical Society; (D) Schematic Illustration of the MIR strategy for DACs^[77]. Copyright 2024, American Chemical Society; (E) Schematic illustration of the synthesis of DACs via a macrocyclic precursor-mediated encapsulation-pyrolysis process. The model on the far right represents the local structure of the M¹M²-DAC^[78]. Copyright 2023, American Chemical Society. DAC: Dual-atom catalyst; SNC: sulfur- and nitrogen-co-doped carbon; MIR: metal ion recognition.

electronegativity can significantly enhance the catalyst's catalytic performance.

Recent in-depth studies on SACs have pointed out that the symmetric M-N₄ structure of traditional SACs, due to its symmetric charge state, is not conducive to the adsorption-desorption and catalytic conversion of all intermediates in catalytic reactions. This results in high reaction barriers and low catalytic selectivity for M-N₄ structure catalysts. Therefore, replacing one of the nitrogen atoms in M-N₄ with other atoms of different electronegativity can impart strong polarity and a special charge state to the metal center, thereby improving its catalytic activity.

Proton exchange membrane fuel cells (PEMFCs) and zinc-air batteries efficiently convert chemical energy into electricity, offering significant promise for new energy vehicles and flexible electronics. However, the sluggish kinetics of the ORR limits their electrocatalytic efficiency. SACs have gained widespread attention due to their fully exposed active sites and high atomic utilization. Current research mainly focuses on symmetric M-N₄ sites anchored on carbon-nitrogen materials. The symmetric M-N₄ sites, due to their uniform electronic distribution, have relatively limited adsorption capability for different intermediates during the ORR process. In contrast, single-atom sites with asymmetric coordination structures exhibit asymmetric electronic distributions, and through effective site regulation, can enhance the adsorption and activation of various intermediate species.

Recently, Li *et al.* synthesized an Fe-N/O-C catalyst featuring isolated Fe-N₃O sites adjacent to vacancy defects^[55]. By introducing O into the first coordination shell and coupling with nearby defects, they tuned the Fe d-orbital energy and spin state from low to intermediate spin, allowing the unpaired dz² electrons to

interact with $O \pi^*$ orbitals to mitigate over-binding [Figure 5A]. The catalyst achieves ORR half-wave potentials of 0.927 V in 0.1 M KOH and 0.80 V in 0.1 M HClO₄ [Figure 5B and C], and zinc–air and PEMFC peak power densities of 490 and 1,179 mW·cm⁻², respectively [Figure 5D]. DFT shows a more negative Fe d-band center in Fe–N/O–C vs. Fe–N–C, weakening intermediate adsorption and shifting the rate-determining step from OH^{*} desorption to OOH^{*} formation. In addition, A coal-pitch-derived Fe SAs/N and S co-doped carbon (NSC)-vacancy defects (vd) catalyst was synthesized via supramolecular self-assembly pyrolysis, yielding asymmetric Fe–N₃S₁ single-atom sites stabilized by abundant vacancy defects^[79]. This vacancy-induced Fe–N₃S₁ coordination synergistically enhances ORR kinetics, delivering markedly improved turnover frequency (TOF) and mass activity in both alkaline and acidic media, far surpassing 20 wt% Pt/C [Figure 5E and F]. Mechanistic analysis indicates that Fe–N sites predominantly facilitate O₂ adsorption activation under alkaline conditions, whereas Fe–S sites govern ORR in acidic media. DFT calculations confirm that the elevated d-band center of Fe–N₃S₁ sites promotes O₂ adsorption and OH reduction, while vacancy defects balance ^{*}OOH formation and ^{*}OH reduction to collectively drive the electrocatalytic ORR. Low-electronegativity boron atoms were introduced by Guan *et al.* to construct an asymmetric Co–N₃B SAC^[80]. Relative to Co–N₄, Co–N₃B reduces ORR free energy and strengthens ^{*}O adsorption, thereby suppressing the two-electron pathway and H₂O₂-induced corrosion to enhance stability. *In situ* attenuated total reflection (ATR)-surface-enhanced infrared absorption spectroscopy (SEIRAS) confirmed robust Co–O intermediate interactions [Figure 5G]. In rechargeable Zn–air batteries, Co–N₃B delivers ≈253 mW·cm⁻² peak power, ≈819 mAh·g⁻¹ energy density, and > 110 h of cycling. Yin *et al.* introduced a P, S co-doping strategy to fine-tune Ce single-atom sites and their N coordination via long-range interactions^[81]. A two-step pyrolysis yielded P,S-modified Ce SAs without oxidation or aggregation. XAS confirmed that N atoms stabilize atomic Ce dispersion [Figure 5H]. The hollow porous carbon polyhedral support further enhances active-site exposure. DFT calculations revealed that P and S shift the Ce-4f orbitals toward the Fermi level, boosting electron transfer. The optimized Ce SAs/PSNC exhibits improved ORR activity and reduced overpotentials. Moreover, there has been some research on constructing asymmetrically coordinated SACs with main group atoms as the center atoms for ORR. Shao *et al.* developed a p-block Sn SAC with axial oxygen ligands to modulate the Sn electronic structure and intermediate adsorption^[82]. The asymmetric Sn SAs achieve an ORR half-wave potential of 0.912 V and a mass activity of 13.1 A·mg_{Sn}⁻¹, outperforming commercial Pt/C and most transition-metal SAs. In both liquid- and solid-state zinc–air batteries, it likewise surpasses Pt/C in electrocatalytic performance. In addition, Lin *et al.* designed an asymmetric Sn–N/O SAC (Sn–N/O–C) that delivers exceptional ORR activity and durability^[83]. In alkaline media, Sn–N/O–C achieves a half-wave potential of 0.910 V, surpassing most state-of-the-art catalysts, and maintains stability in both alkaline and acidic electrolytes. In Zn–air batteries, it affords an energy density of 254 mW·cm⁻², outperforming reported M–N–C cathodes. DFT calculations reveal that asymmetric N,O coordination strengthens O₂ adsorption and charge transfer vs. symmetric SnN₄ sites, thereby accelerating ORR process [Figure 5I]. This work establishes an N/O coordination strategy for crafting robust, high-performance p-block metal single-atom ORR catalysts.

Electrochemical CO₂ reduction into fuels or value-added chemicals offers a promising route to mitigate energy and environmental challenges, garnering extensive interest from both academia and industry. Nevertheless, sluggish CO₂ activation kinetics and the scarcity of efficient electrocatalysts necessitate high energy inputs, impeding industrial deployment. Consequently, designing electrocatalysts with enhanced activity and selectivity is critical. Transition-metal SACs supported on N-doped porous carbon have demonstrated considerable advancement in CO₂ electro conversion, yet their symmetric atomic coordination constrains catalytic performance. Precisely tuning the atomic-level coordination environment to optimize intermediate adsorption and facilitate charge transfer to the single-atom active sites remains a formidable challenge. Recently, Huang *et al.* employed Mg(OH)₂ as a low-cost template, whose decomposition during pyrolysis generated water vapor for axial Ni–O coordination, while ammonia doping

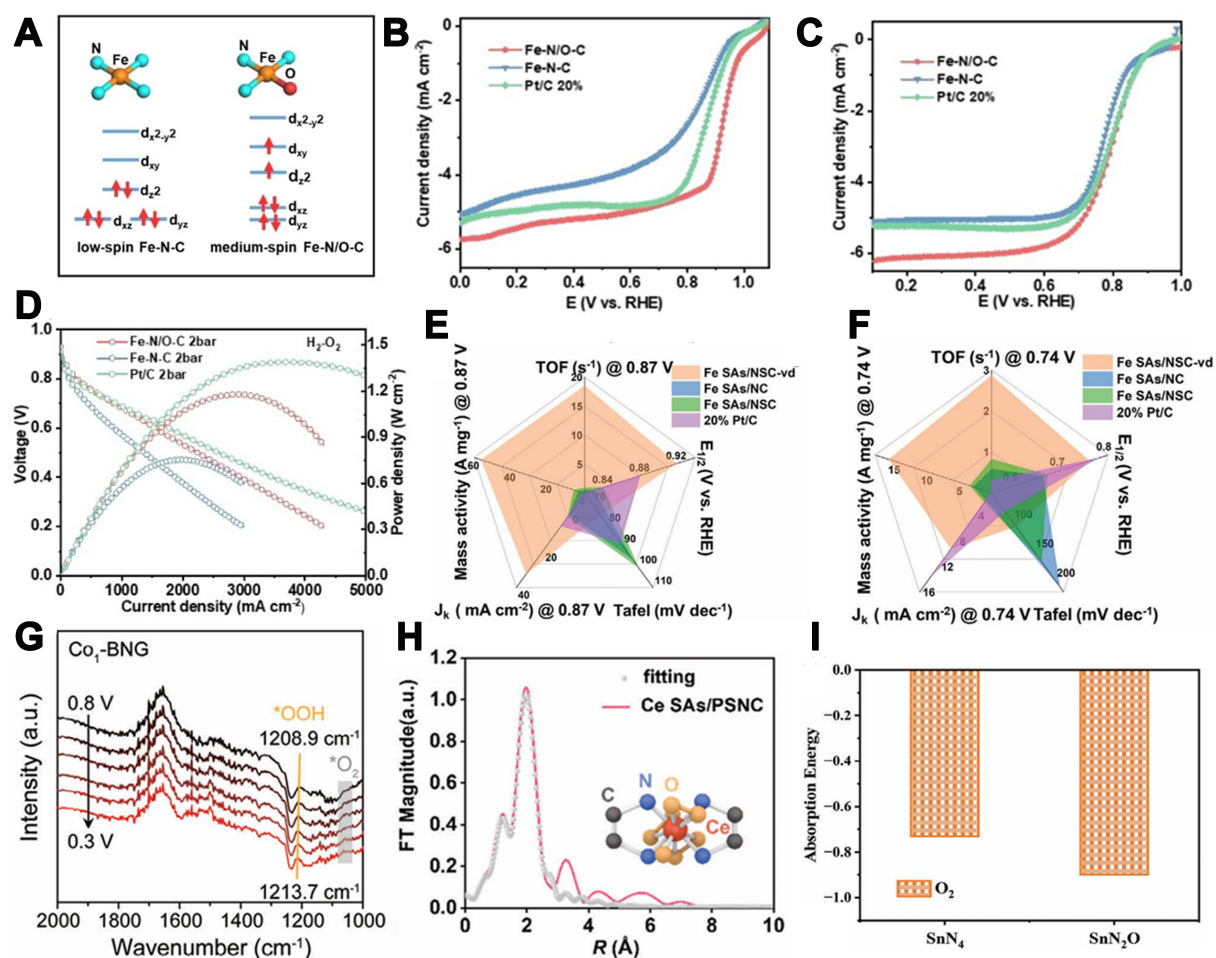


Figure 5. (A) Schematic diagram of d-orbital spin-electron filling states; (B) LSV curves of FeN/OC, FeNC and Pt/C 20% in 0.1 M KOH at the rotation speed of 1,600 rpm; (C) LSV curves of FeN/OC, FeNC and Pt/C 20% in 0.1 M HClO₄ at the rotation speed of 1,600 rpm; (D) Polarization curves and corresponding power density plots of FeN/OC, FeNC and Pt/C-assembled 2.0 bar H₂-O₂ PEMFCs. Copyright 2024, Wiley-VCH; (E) $E_{1/2}$, J_k , Tafel, mass activity, and TOF at 0.87 V of the catalysts in 0.1 M KOH and (F) 0.5 M H₂SO₄. Copyright 2024, Wiley-VCH; (G) *In situ* ATR-SEIRAS spectra of ORR over Co₁/BNG in O₂-saturated 0.1 M KOH. Copyright 2024, Wiley-VCH; (H) The corresponding EXAFS R-space fitting curves of CoSAs/PSNC. Copyright 2023, Wiley-VCH; (I) O₂ absorption energies on the optimized model structures of SnN₄ and SnN₂O. Copyright 2024, Wiley-VCH. LSV: Linear sweep voltammetry; PEMFCs: proton exchange membrane fuel cells; TOF: turnover frequency; ATR-SEIRAS: attenuated total reflection-surface-enhanced infrared absorption spectroscopy; ORR: oxygen reduction reaction; EXAFS: extended X-ray absorption fine structure.

formed lateral Ni-N₄ sites on porous graphitic carbon^[84]. The resulting Ni SA-N-PGC catalyst, featuring asymmetric Ni-N₄-O coordination, achieved over 97% CO Faradaic efficiency (FE) at -0.76 V (9,097 h⁻¹) and maintained > 90% efficiency across -0.5 to -1.1 V, with negligible decay after 40 h. Mechanistic studies revealed that axial Ni-O coordination induced site asymmetry, optimized the local coordination environment, enhanced charge polarization, and lowered the Gibbs free energy of *COOH formation, thereby improving ORR kinetics and selectivity [Figure 6A and B]. Jin *et al.* designed an asymmetric Fe-S₁N₃ SAC, where one Fe atom is coordinated to one S and three N atoms, inducing pronounced geometric distortion^[85]. The Fe-S₁N₃ site dynamically adjusts its structure upon intermediate adsorption, decoupling *COOH and *CO binding energies and breaking their linear scaling relation. This structural adaptability yields a CO FE of 99.02% and a TOF of 7,804 h⁻¹, alongside robust stability. Furthermore, Wang *et al.* pointed out that main group SACs have the ability to prevent hydrogen evolution reactions (HER) and CO poisoning, making them promising for CO₂RR to produce CO^[86]. Based on this, the researchers

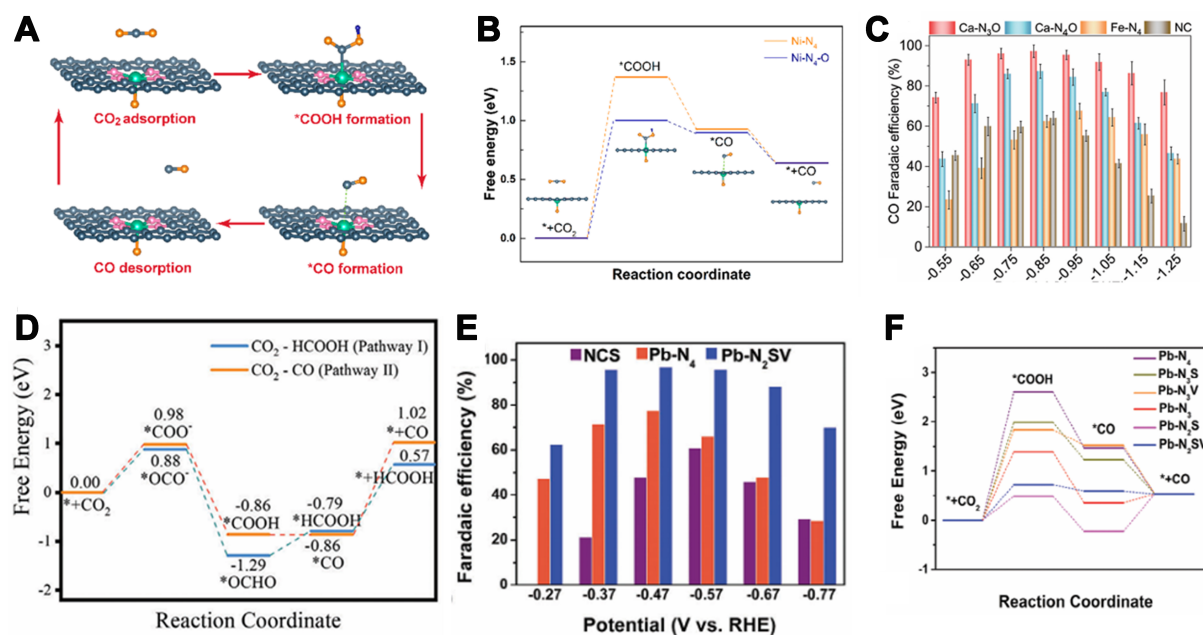


Figure 6. (A) Proposed reaction steps of electrocatalytic reduction of CO₂ to CO over the Ni-N₄-O catalytic site; (B) Reaction paths and free energy diagrams of CO₂ reduction to CO over Ni-N₄ and Ni-N₄-O catalytic sites. Inset shows the side view of the optimized configurations of intermediates over the Ni-N₄-O catalytic site^[84]. Copyright 2022, American Chemical Society; (C) FE_{CO} at different potentials in H-cell^[86]. Copyright 2023, Wiley-VCH; (D) The Gibbs free energy diagrams of pathways I (from CO₂ to HCOOH) and II (from CO₂ to CO)^[87]. Copyright 2024, Wiley-VCH; (E) Comparison of FE_{CO} at different potentials for NCS, Pb-N₄ and Pb-N₂SV in CO₂-saturated 0.5 M KHCO₃; (F) Gibbs free energy profiles^[88]. Copyright 2024, Wiley-VCH. FE_{CO}: CO Faradaic efficiency; NCS: sulfur- and nitrogen-co-doped carbon.

reported an O-doping strategy that formed an asymmetric coordination structure (Ca-N₃O) around Ca atoms, which localized electrons on the p-orbital, thus enhancing CO₂ activation. Combining DFT calculations and experimental verification, they confirmed the advantages of the asymmetric coordination structure in CO₂ activation and *COOH generation. This catalyst exhibited excellent catalytic activity and selectivity in the CO₂ reduction to CO reaction. As shown in Figure 6C, the FE for CO was as high as 97.3% at -0.85 V [vs. reversible hydrogen electrode (RHE)], and in the flow cell, a high current density of 400 mA·cm⁻² was achieved while maintaining an FE of ≥ 90%. Liu *et al.* used a rapid pulsed discharge to fabricate a graphene-aerogel-supported Cu SA catalyst (CuN₁O₁-SAs/GAs)^[87]. The intense thermal shock and electromagnetic field drove *in situ* N-doping and atomic dispersion of Cu, yielding an asymmetric Cu-N₁O₁ coordination confirmed by atomic-level analysis. CuN₁O₁-SAs/GAs displayed high selectivity and activity for HCOOH production across a wide potential range in CO₂RR, with stable current densities over 10 h. *In situ* XAFS showed elongated Cu-N/O bonds that facilitate formate formation, and DFT calculations indicated a lower energy barrier for HCOOH vs. CO and a preference for HCOOH at unsaturated Cu-N₁O₁ sites [Figure 6D]. Notably, although bulk p-block metals (e.g., Pb, Bi) favor CO₂-to-HCOOH conversion, their single-atom analogs often exhibit enhanced CO selectivity due to fully occupied d-orbitals. Moreover, Zhou *et al.*, guided by DFT calculations, designed a novel Pb SAC (Pb-N₂SV), in which Pb is coordinated to two N atoms, one S atom, and an adjacent vacancy, creating a highly asymmetric microenvironment^[88]. This symmetry breaking endowed Pb-N₂SV with superior CO₂ electroreduction activity at -0.47 V, achieving a CO FE of 97.3% [Figure 6E] and stable operation over 33 h, surpassing most p-block SACs. *In situ* IR and DFT analyses indicate that S doping enhances electron localization at the Pb center, promoting *COOH adsorption, while vacancy defects modulate electronic dispersion to facilitate *CO desorption [Figure 6F]. These synergistic effects optimize intermediate adsorption energies and accelerate CO₂RR.

Multi-metal asymmetric coordination structures

In complex multistep reactions, the adsorption and desorption strengths of various intermediates at the active sites are often different. However, SACs feature only a single active center and therefore exhibit the same adsorption/desorption response for all intermediates. Therefore, multi-metal asymmetric coordination structures have been introduced into electrochemical systems with multiple reaction intermediates (e.g., ORR, OER, NRR, CO₂RR^[40,67,68,73]), enabling differentiated control over each intermediate's adsorption and desorption behavior. Multi-metal asymmetric coordination structures can effectively regulate the charge state, orbital energy levels, d-band center, optimize electronic spin configurations, and influence the bonding and antibonding states of reactants, thus optimizing the adsorption and desorption of intermediates during the reaction. Moreover, multi-metal sites enable tandem catalysis during the reaction process. Different active site centers can achieve optimal adsorption and desorption capabilities for various intermediates, allowing the reaction to proceed smoothly^[89–91]. In this section, we will discuss the applications of multi-metal asymmetric coordination structures in ORR and CO₂RR.

As shown in [Figure 7A](#), Li *et al.* synthesized a Cu-Co/NC catalyst with outstanding bifunctional ORR/OER activity in alkaline media (ORR $E_{1/2}$ = 0.92 V), and maintained strong ORR performance in acidic (0.85 V) and neutral (0.74 V) electrolytes^[65]. When applied in zinc–air batteries, it delivered stable open-circuit voltage, polarization, and power density, and endured 1,000 charge-discharge cycles (510 h at 10 mA·cm^{−2}) without performance loss. DFT analysis revealed that Cu-Co dual sites induce asymmetric charge distribution, optimizing adsorption/desorption of oxygen intermediates and accelerating both ORR and OER kinetics. It is noteworthy that diatomic catalysts composed of two identical metal atoms likewise exhibit high catalytic activity. Li *et al.* synthesized a charge-asymmetric dual-atom catalyst Fe₂-S₁N₅/SNC using a two-step method^[92]. Fe₂-S₁N₅/SNC exhibited excellent electrocatalytic performance in acidic flow cells. In 0.1 mol·L^{−1} HClO₄ solution, its half-wave potential reached 0.829 V, an improvement of 56 mV compared to the SAC Fe-N₄/NC. When loaded on the cathode of a hydrogen fuel cell, it demonstrated a high peak power density of 810 mW·cm^{−2} [[Figure 7B](#)]. The authors attributed the catalyst's excellent performance to the fact that charge-asymmetric dual-atom sites can more flexibly regulate the adsorption energy of point-charged intermediates at the active center, and the asymmetric electronic structure enhances the electronic transfer capability. In 2024, He *et al.* synthesized Co-Fe-SNC via a host–guest strategy to create bridging asymmetric Co-Fe coordination^[93]. Atomically dispersed Co-Fe sites, combined with sulfur-driven surface modulation, deliver superior ORR performance, achieving a half-wave potential of 0.92 V in alkaline media [[Figure 7C](#)]. DFT studies reveal that bimetallic sites strengthen oxygen-intermediate binding and lower activation barriers, while sulfur's weak electronegativity fine-tunes the electronic structure for further activity enhancement. Employed as zinc–air battery cathodes, Co-Fe-SNC surpasses commercial Pt/C in power density, specific capacity, and durability. It is worth noting that Li *et al.* engineered a Fe-Ru dual-atom catalyst on N-doped carbon with moderate tensile strain, achieving record acidic ORR performance among Fe SACs^[94]. Strain-tuned d-band center yielded a half-wave potential of 0.86 V and a fuel-cell power density of 700 mW·cm^{−2}. After 50,000 cycles, the half-wave potential dropped by only 17 mV, demonstrating exceptional durability. *In situ* SEIRAS and DFT analyses reveal that tensile strain enhances d-electron penetration into antibonding orbitals, accelerating intermediate reduction and desorption. ATR-SEIRAS further confirmed strain-optimized Fe-O bonding and faster ORR kinetics in acid.

Furthermore, asymmetric catalysts utilizing metal oxides as supports have likewise demonstrated superior ORR performance. For example, Li *et al.* successfully synthesized a PdCu-Fe₃O₄ in-plane heterostructure through sequential reduction of different metal precursors^[95]. This structure combines the advantages of Pd and Fe₃O₄, achieving synergistic catalysis. The authors pointed out that this method ensures the uniformity

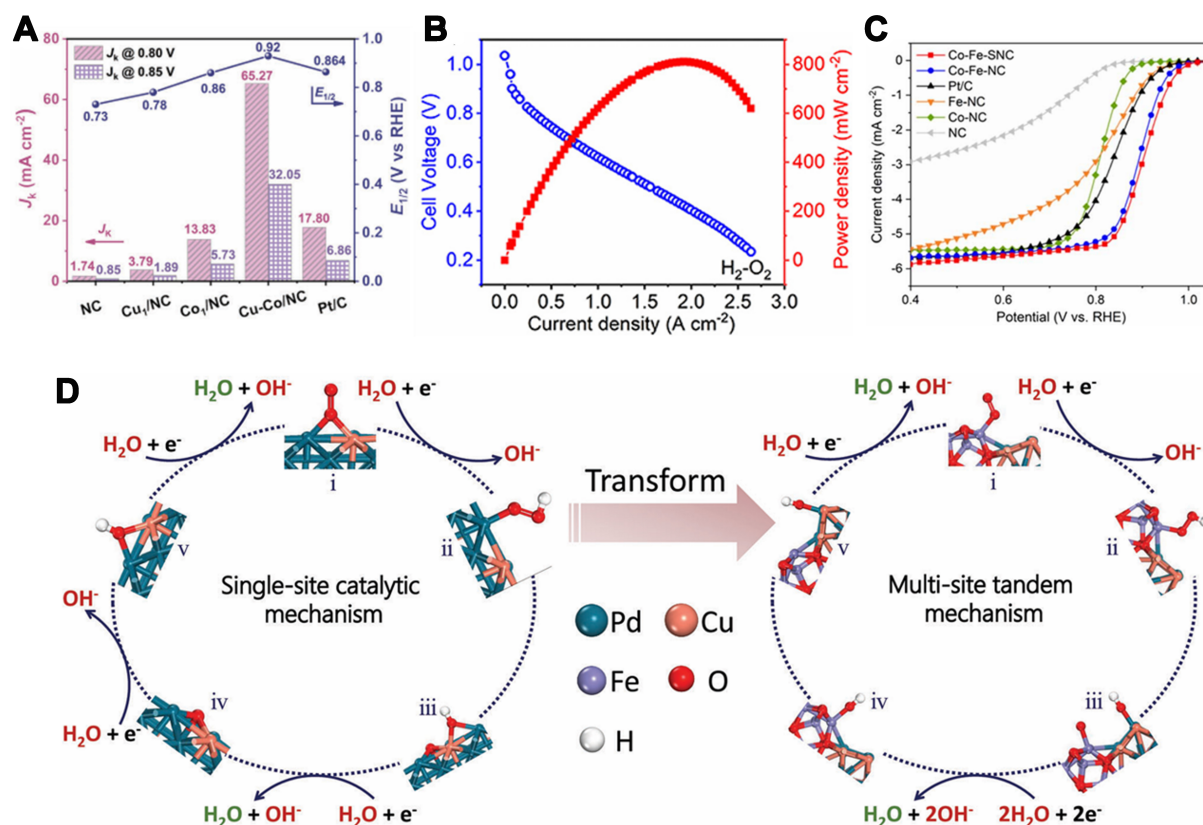


Figure 7. (A) Kinetic current density of electrocatalysts at 0.80 and 0.85 V^[65]. Copyright 2023, Wiley-VCH; (B) PEMFC polarization and power density curves of Fe₂-S₄N₅N₃/SNC^[92]. Copyright 2024, The Royal Society of Chemistry; (C) LSV polarization curves of the ORR in O₂-saturated 0.1 M KOH solution^[93]. Copyright 2024, The Royal Society of Chemistry; (D) Schematic illustration of the single-site catalytic mechanism for PdCu (left) and multi-site tandem mechanism for PdCu-Fe₃O₄ (right)^[95]. Copyright 2024, Wiley-VCH. PEMFC: Proton exchange membrane fuel cell; LSV: linear sweep voltammetry; ORR: oxygen reduction reaction.

and stability of the heterostructure. ORR catalytic performance evaluation of the prepared PdCu-Fe₃O₄ in-plane heterostructure showed that it maintained close to 4e⁻ electron transfer numbers at different potentials, indicating its high catalytic activity. Notably, the study found that the proton-coupled electron transfer (PCET) steps during ORR occur in an orderly manner at Pd and Fe sites. The initial PCET steps occur at Fe sites, while the last two PCET steps take place at the optimal Pd sites [Figure 7D]. This reveals the tandem catalysis mechanism of ORR on the PdCu-Fe₃O₄ in-plane heterostructure, providing a new research paradigm for understanding ORR mechanisms in complex systems.

Remarkably, catalysts featuring multi-metal asymmetric coordination structures also find extensive applications in the CO₂RR. For example, Zhu *et al.* constructed a quasi-covalently bonded Ni-Cu dual-atom electrocatalyst (Ni/Cu-N-C) exhibiting exceptional CO₂ reduction performance^[69]. It delivers peak current densities and the lowest onset potential across the full potential window, achieving 13.7 mA cm^{-2} at -0.7 V (vs. RHE) - 3.8 and 5.9 times those of Ni-N-C and Cu-N-C, respectively [Figure 8A]. Ni/Cu-N-C maintains $\geq 97.7\%$ FE throughout, with $j_{(\text{co})}$ of 24.8 mA cm^{-2} at -0.8 V and an unprecedented TOF of 20,695 h^{-1} at -0.6 V [Figure 8B]. It shows stable current and efficiency over 60 h. *In situ* XAFS indicates that Cu accelerates CO₂-CO conversion and prevents Ni over-reduction, boosting site stability. DFT/NBO analyses reveal that Ni-C antibonding states in NiCuN₆ sites raise *COOH adsorption via Ni 3d-C 2p hybridization and stronger Ni-C σ bonding, underpinning superior intrinsic activity [Figure 8C and D]. As shown in Figure 8E, Chen *et al.* designed a Cu atom fixed on an N, S-doped carbon matrix for CO₂RR, Cu₂-NC^[96]. The results showed

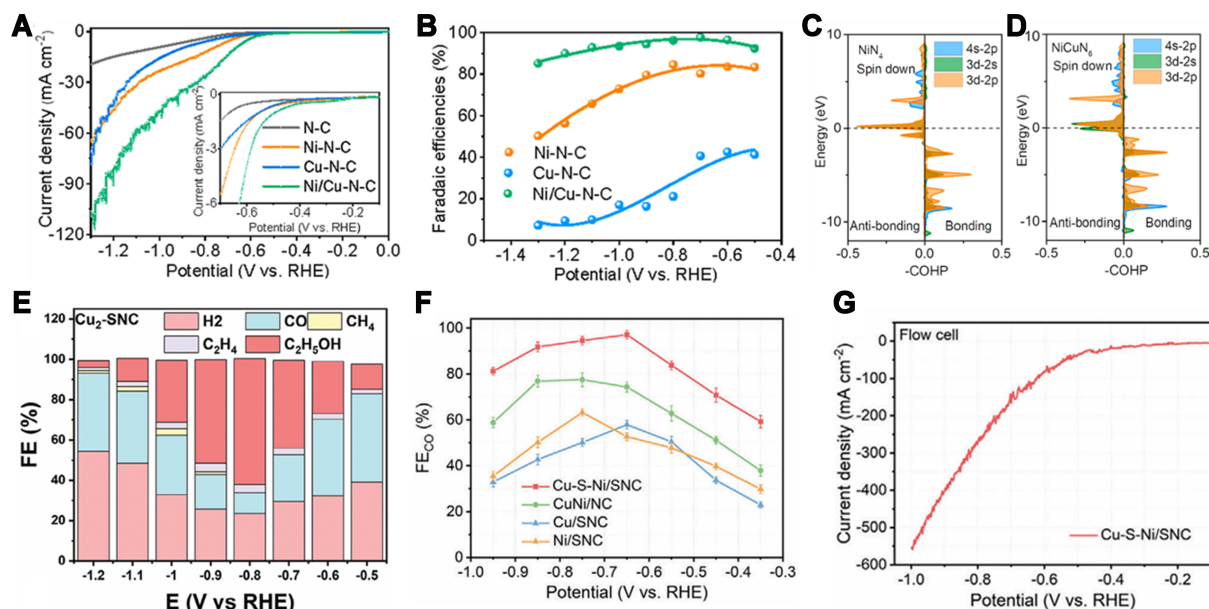


Figure 8. (A) LSV curves acquired in CO₂-saturated 0.5 M KHCO₃ solution on a rotating disc electrode at a rotating speed of 1,600 rpm. The inset highlights the LSV curves in the potential range from -0.1 to -0.7 V; (B) FE for CO production at various applied potentials; (C and D) COHP analysis of the Ni-C bond on NiN₄ and NiCuN₆; note that -COHP is used as the a-axis^[69]. Copyright 2022, American Chemical Society; (E) FE value at different potentials by Cu₂-SNC catalysts^[96]. Copyright 2024, Wiley-VCH; (F) FE_{CO} at different potentials of Cu-S-Ni/SNC and references; (G) LSV curves of Cu-S-Ni/SNC in the flow cell^[75]. Copyright 2024, Wiley-VCH. LSV: Linear sweep voltammetry; FE: Faradaic efficiency; COHP: crystal orbital Hamilton population; SNC: sulfur- and nitrogen-co-doped carbon.

that Cu₂-SNC exhibited extraordinary and stable electrocatalytic performance for CO₂-ethanol conversion (with FE of 62.6% at -0.8 V vs. RHE), far outperforming Cu-NC and Cu₂-NC. DFT calculations revealed the reaction mechanism for the high selectivity of ethanol and were further confirmed by *in situ* attenuated total reflection Fourier transform infrared (ATR-FTIR) spectroscopy. The asymmetric electronic cloud distribution around Cu dual-atom sites in CuN₂-CuNS destabilizes ethylene reaction intermediates, thus favoring ethanol formation. Similarly, Sun *et al.* fabricated a sulfur-bridged asymmetric CuNi dual-atom site catalyst, Cu-S-Ni/SNC, which exhibited excellent CO₂RR performance in an H-type cell, with a CO Faradaic efficiency (FE_{CO}) of 98.1% at -0.65 V^[75]. In a flow cell, the industrial current density reached 550 mA·cm⁻² [Figure 8F and G]. The high performance of Cu-S-Ni/SNC is due to the electronic tuning effect between Cu and Ni through the sulfur bridge, where electrons transfer from Cu to Ni. *In situ* spectroscopy and DFT calculations showed that Cu, as the primary adsorption site, is doubly regulated by S and Ni atoms, with Ni and S atoms enhancing Cu's CO₂ activation and the formation of the *COOH intermediate. The study showed that adjusting the type of bridging atom can effectively modulate the charge state of asymmetric sites, which is beneficial for CO₂RR development.

CHARACTERIZATION METHODS FOR ASYMMETRIC COORDINATION STRUCTURES

In the rapidly expanding domain of multi-scale design for single-atom catalysis, a thorough grasp of the subtle structural characteristics inherent in catalytic materials is essential for achieving exceptional catalytic performance. At the nanoscale and below, the intricate organization of atoms and molecules plays a fundamental role in determining the catalytic activity, selectivity, and longevity of SACs. To decipher these intricate structural, morphological, and electronic properties, advanced characterization techniques are indispensable. This section outlines key advanced characterization techniques: aberration-corrected STEM coupled with electron energy-loss spectroscopy (EELS), XAS, and time-of-flight secondary ion mass spectrometry (ToF-SIMS).

Aberration-corrected scanning transmission electron microscopy with electron energy loss spectroscopy

Electron microscopy techniques, including scanning electron microscopy (SEM), transmission electron microscopy (TEM), and HRTEM, have been widely used for morphology characterization of catalysts. However, they are limited by insufficient resolution and thus cannot accurately characterize individual atoms. To address this limitation, aberration-corrected scanning transmission electron microscopy (AC-STEM) has been developed to observe single atoms. In particular, spherical aberration-corrected HAADF-STEM (AC-HAADF-STEM) can display larger metal atoms as prominent bright spots. This allows for the observation of single-atom sites and dual-atom sites in catalyst materials. Sun *et al.* used AC-HAADF-STEM to characterize the Cu-S-Ni/SNC catalyst they prepared, as shown in Figure 9A, where the yellow circles highlight isolated bimetallic sites, and the red circles encircle individual Cu or Ni single atoms^[75]. Figure 9B shows the 3D model of the dual-atom site at position 1 in Figure 9A. The authors statistically analyzed most of the sites in the image, and the results showed that bimetallic sites accounted for more than 70% [Figure 9C], confirming that Cu-Ni bimetallic sites dominate in the catalyst. Similarly, Xie *et al.* used AC-HAADF-STEM to confirm that most of the Zn-Fe metals in their prepared Fe-Zn@SNC catalyst exist as isolated dual-atom sites (as shown in the yellow circle in Figure 9D)^[97]. Furthermore, the authors statistically analyzed the distance between the dual-atom sites, and the results Figure 9E showed that the distance between dual-atom sites in Fe-Zn@SNC catalyst is primarily concentrated between 2.8 to 3.3 Å.

However, AC-STEM cannot provide information on the chemical composition and elemental identification of the sample, which is complemented by EELS. In recent years, EELS has offered unparalleled advantages for the characterization of SACs and DACs. By measuring the energy-loss spectrum of a high-energy electron beam transmitted through a specimen, EELS yields rich information about elemental composition, chemical bonding, oxidation state and coordination environment^[98]. When combined with aberration-corrected high-resolution scanning transmission electron microscopy (STEM), it enables sub-angstrom localization of individual atoms, while the energy-loss spectrum confirms elemental identity and discriminates impurity atoms. This structural–chemical dual-criterion approach permits both qualitative and quantitative determination of atomic positions and oxidation states, thereby effectively eliminating misidentification^[99–101]. The STEM–EELS tandem thus provides significant advantages in active-site identification of SA catalysts, elemental qualitative–quantitative analysis, microstructural characterization and *in situ* dynamic observation. Zhang *et al.* used HAADF-STEM to characterize the FeCu bimetallic catalyst they prepared (the schematic structure of which is shown in Figure 10A)^[78]. Figure 10B shows a large number of bright spots dispersed on the carbon support, which are considered to be metal sites. The researchers pointed out that the proportion of metal atom pairs is about 70%. Additionally, the authors performed EELS analysis on the atomic pair within the red box in Figure 10B, and the results, shown in Figure 10C, confirmed that the two bright spots within the red box are Fe-Cu atomic pairs. As shown in Figure 10D, Yang *et al.* undertook a two-phase method to create Cu-N-C SACs, featuring a uniform and distinctly defined Cu²⁺-N₄ configuration^[102]. It is also confirmed the dispersion of Cu atoms by observing HAADF-STEM images [Figure 10E], and the clear signals of C, N, and Cu in EELS, combined with elemental mapping, further corroborated the N/C coordination [Figure 10F]. Despite the single-atom sensitivity of AC-STEM with EELS and its capability to obtain rich physicochemical properties, the requirement for sample stability under the electron beam necessitates the combination of other characterization techniques for analysis^[98].

XAS

Synchrotron radiation XAS plays a crucial role in the study of asymmetric coordination structures. XAS includes extended XANES and extended XAFS (EXAFS). XANES can provide information on the atomic electronic orbitals and oxidation states in SACs, as well as the electron density distribution, oxidation state

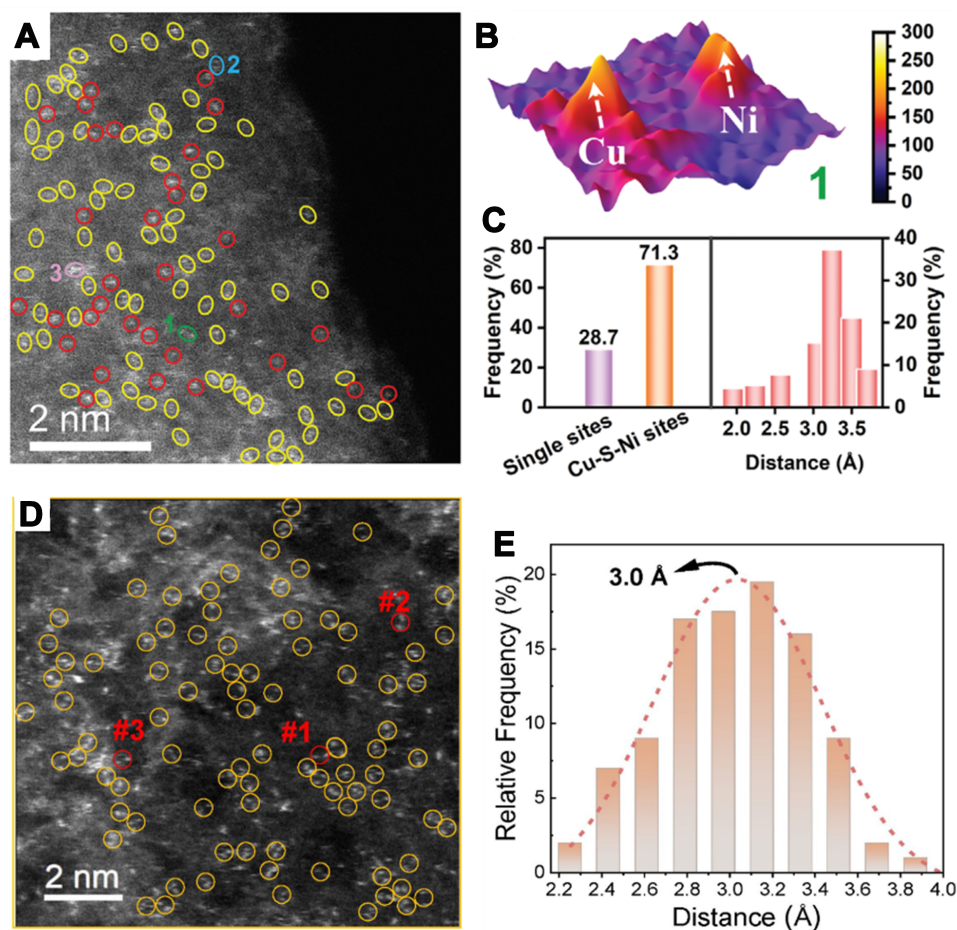


Figure 9. (A) HAADF-STEM image of Cu-S-Ni/SNC. The dual-atom sites and single sites were circled with dotted yellow line and red line, respectively; (B) 3D model of Cu-S-Ni sites along the region of 1 in (A); (C) Density profiles of Cu-S-Ni and single-atom sites in the HAADF-STEM^[75]. Copyright 2024, Wiley-VCH; (D) HAADF-STEM image of Fe-Zn@SNC; (E) Kernel method of frequency statistic and Gauss fitting of diatomic distances obtained from all the yellow circles in (D)^[97]. Copyright 2023, Wiley-VCH. HAADF-STEM: High-angle annular dark-field scanning transmission electron microscopy; SNC: sulfur- and nitrogen-co-doped carbon.

changes, and the localization of electrons in single atoms. This is particularly important for analyzing the electron transfer processes in catalytic reactions. On the other hand, EXAFS can reveal the local structure of single atoms in detail, including coordination environment, bond lengths, and coordination numbers, which can help researchers understand the arrangement of surrounding atoms in SACs. Furthermore, by utilizing the high temporal resolution capabilities of synchrotron radiation XAS, researchers can monitor the dynamic changes of SACs in real-time during catalytic reactions, capturing the evolution of their structure and electronic states at different stages of the reaction^[103-107]. Additionally, the high temporal resolution of synchrotron radiation XAS allows researchers to monitor the dynamic changes of SACs during catalytic reactions in real time, capturing the evolution of their structure and electronic states at different stages of the reaction.

As shown in Figure 11A, Pei *et al.* investigated the local coordination environment of Co-S_xN_{4-x} SACs using XANES and FT-EXAFS techniques^[108]. The XANES spectra revealed that, compared to Co foil and Co₃O₄, the Co in SACs carries a positive charge and exhibits a lower valence state, which decreases as the S content increases. FT-EXAFS analysis [Figure 11B] confirmed the single-atom structure of Co and unveiled a new

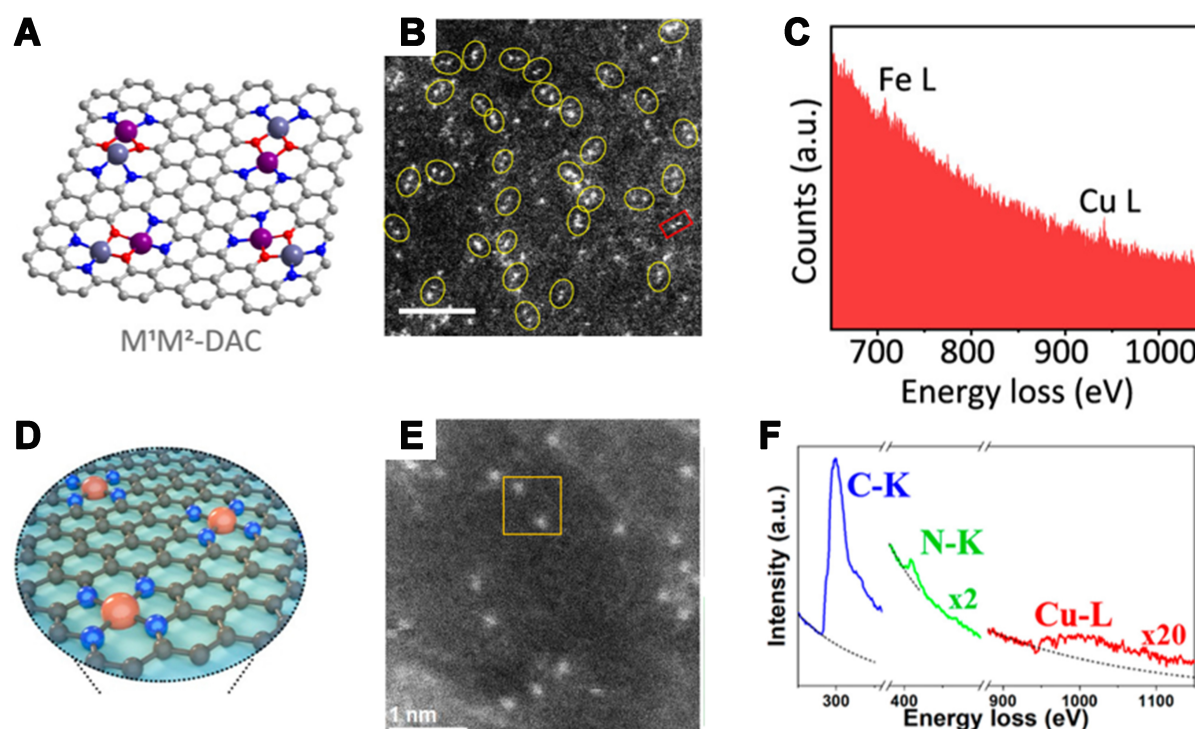


Figure 10. (A) The local structure of the M^1M^2 -DAC; (B) HAADF-STEM image of FeCu-DAC; (C) EELS of an Fe-Cu atomic pair as marked in the red rectangle in the HAADF-STEM image^[78]. Copyright 2023, American Chemical Society; (D) The structure of Cu-N-C SAC; (E) Atomic-resolution STEM-HAADF image; (F) The EELS extracted from the yellow rectangle in STEM-HAADF image^[102]. Copyright 2021, American Chemical Society. DAC: Dual-atom catalyst; HAADF-STEM: high-angle annular dark-field scanning transmission electron microscopy; EELS: electron energy-loss spectroscopy; SAC: single-atom catalyst.

Co-S scattering peak that intensifies with increasing S content. Through EXAFS fitting [Figure 11C-F], researchers extracted structural parameters, finding that an increase in Co-S coordination number leads to a decrease in Co-N coordination number, indicating the substitution of N by S.

Similarly, Sun *et al.* studied the local coordination structure of the Cu-S-Ni asymmetric sites in Cu-S-Ni/SNC catalysts using XANES and EXAFS techniques [Figure 12A]^[75]. Figure 12B and C shows the normalized Cu and Ni K-edge XANES spectra of Cu-S-Ni/SNC and comparative samples. The results show that Cu in Cu-S-Ni/SNC has a higher oxidation state compared to Cu foil, presenting a positive oxidation state, but its oxidation state lies between that of CuNi/NC and Cu/SNC, indicating that the oxidation state of Cu is influenced by Ni and S elements. Similarly, the Ni K-edge XANES spectrum shows that Ni in Cu-S-Ni/SNC also exhibits a positive oxidation state, with its oxidation state between that of CuNi/NC and Ni/SNC, which is mainly due to the effect of the coordination environment and the doping elements [Figure 12C]. These observations suggest that the electronic oxidation states of Cu and Ni are both between 0 and +2, and are influenced by the S atoms and the second metal.

EXAFS spectra elucidate local atomic coordination in Cu-S-Ni/SNC. Cu K-edge data [Figure 12D] feature a main Cu-N peak at 1.65 Å, a Cu-S shoulder at 1.85 Å, and a minor Cu-Ni signal at 2.62 Å - longer than the 2.47 Å direct Cu-Ni bond. Ni K-edge spectra [Figure 12E] show analogous peaks at 1.72 Å (Ni-N) and 1.92 Å (Ni-S), plus a Ni-Cu scattering at ~2.5 Å. The metallic scattering signatures confirm Cu-Ni interactions and the modulatory effect of S ligands on electronic structure, providing a structural basis for the catalyst's synergistic effects and enhanced performance.

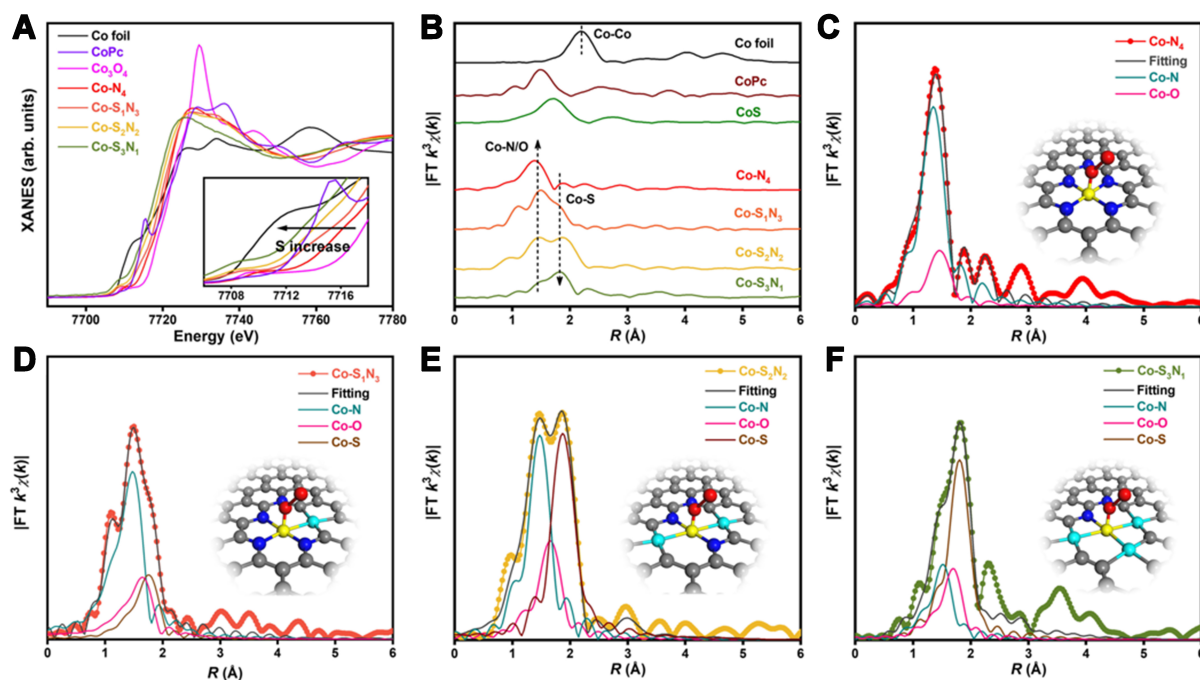


Figure 11. (A) XANES and (B) FT-EXAFS spectra of the $\text{Co-S}_x\text{N}_{4-x}$ SACs; (C) Co-N_4 ; (D) $\text{Co-S}_1\text{N}_3$; (E) $\text{Co-S}_2\text{N}_2$ and (F) $\text{Co-S}_3\text{N}_1$ [108]. Copyright 2021, Springer Nature. XANES: X-ray absorption near edge structure; FT-EXAFS: Fourier transform extended X-ray absorption fine structure; SACs: single-atom catalysts.

To elucidate the true active sites and their dynamic evolution, the authors employed *in situ* XAS spectroscopy to monitor the catalytic behavior of Cu-S-Ni/SNC [Figure 12F-I]. Upon exposure to CO_2 -saturated KHCO_3 , the Cu K-edge XANES shifts +1.05 eV, indicating CO_2 adsorption-induced charge transfer and oxidation of Cu sites, while the Ni K-edge shifts -0.48 eV, suggesting Ni acts as an electron acceptor to modulate Cu's oxidation state. Under applied potential, both Cu and Ni pre-edge peaks shift to lower binding energies, indicating progressive reduction; in Cu K-edge FT-EXAFS, the Cu-N bond contracts from 1.62 to 1.55 Å and Cu-S from 1.85 to 1.78 Å, with analogous shifts observed in the Ni EXAFS. From these observations, the authors conclude that Cu atoms serve as the principal active sites for CO_2 reduction, and that S-derived electrons, coupled into the Cu/Ni 3d orbitals, synergistically enhance Cu's adsorption and catalytic performance.

ToF-SIMS

ToF-SIMS is an advanced analytical technique that bombards a sample with high-energy ions to sputter secondary ions, which are then separated based on their mass-to-charge ratios. ToF-SIMS, as a static SIMS technique, allows for re-analysis of the sample surface without causing destruction. The mass spectra obtained not only encompass atomic ions but also include molecular ions unique to the original surface, providing richer molecular information compared to XPS and boasting higher resolution [109].

Koshy *et al.* synthesized Ni-N-doped carbon materials, which are designed as electrocatalysts for CO_2 reduction [110]. The critical information regarding the presence and distribution of NiN_xC_y fragments gathered through the ToF-SIMS provided definitive evidence for the existence of isolated, nitrogen-coordinated single nickel atom sites. Specifically, within a Ni-N-C material derived from pyrolyzed polyacrylonitrile (NiPACN), a clear peak corresponding to the $^{58}\text{NiN}_2\text{C}_2^-$ fragment was detected at 109.94 amu. Notably, no peak appeared within the same mass range in the metal-free PACN control, providing

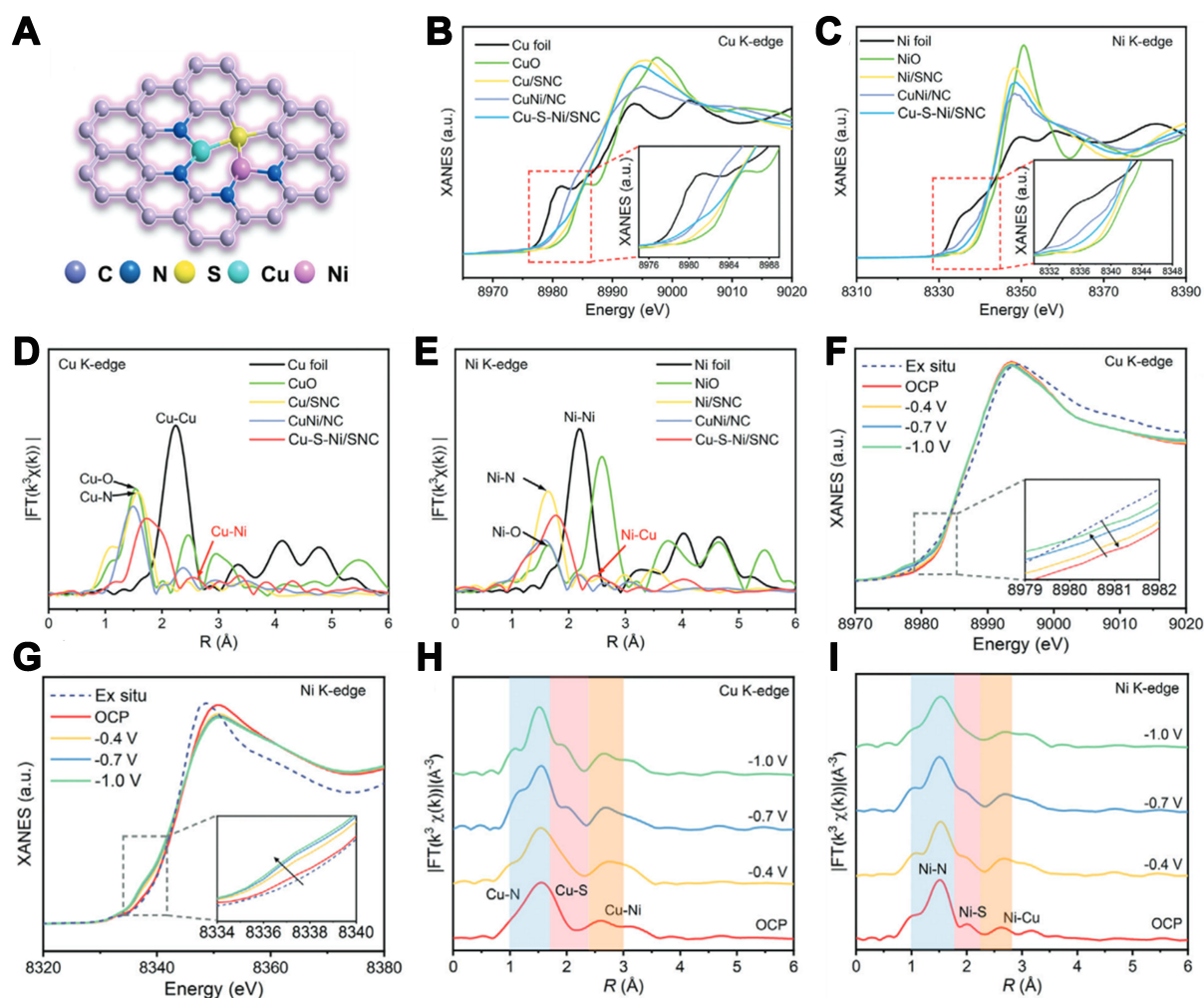


Figure 12. (A) Atomic structure model of Cu-S-Ni/SNC; (B) The Cu K edge XANES spectra of Cu-S-Ni/SNC; (C) The Ni K edge XANES spectra of Cu-S-Ni/SNC; (D) The Cu K edge FT-EXAFS spectra of Cu-S-Ni/SNC and the references; (E) The Ni K edge FT-EXAFS spectra of Cu-S-Ni/SNC and the references; (F) The Cu K-edge XANES spectra of Cu-S-Ni/SNC at various potentials during CO_2RR ; (G) The Ni K-edge XANES spectra of Cu-S-Ni/SNC at various potentials during CO_2RR ; (H) The Cu K-edge FT-EXAFS at open circuit, -0.4, -0.7, and -1.0 V vs. RHE; (I) The Ni K-edge FT-EXAFS at open circuit, -0.4, -0.7, and -1.0 V vs. RHE^[75]. Copyright 2024, Wiley-VCH. SNC: Sulfur- and nitrogen-co-doped carbon; XANES: X-ray absorption near edge structure; FT-EXAFS: Fourier transform extended X-ray absorption fine structure; RHE: reversible hydrogen electrode.

compelling evidence that the NiN_2C_2^- fragment originates from NiPACN [Figure 13A]. Similarly, a peak for NiPACN, corresponding to the anticipated and confirmed presence of the ^{60}Ni isotope fragment $^{60}\text{NiN}_2\text{C}_2^-$, was observed at approximately 111.94 amu, which was absent in the PACN sample [Figure 13B].

The study by Mukadam *et al.* also employed ToF-SIMS as a key analytical technique, in which ToF-SIMS was used to investigate the surface composition and stability of phthalocyanine-based single-atom Co/CuPc catalysts during the electrochemical reduction of furfural^[111]. By analyzing the changes in the total ion counts of Co Pc and Cu Pc before and after the constant potential testing, it was found that the normalized count of Co Pc decreased by 16% [Figure 13C], indicating the stability of Co Pc towards furfural reduction. In contrast, for Cu Pc, the normalized counts of Cu^+ and Cu Pc⁺ decreased by 67% and 69%, respectively [Figure 13D], suggesting that Cu Pc was removed. Therefore, Cu Pc exhibits less stability towards furfural reduction compared to Co Pc. Zhang *et al.* employed ToF-SIMS to probe FeCu-DAC by analyzing ion-

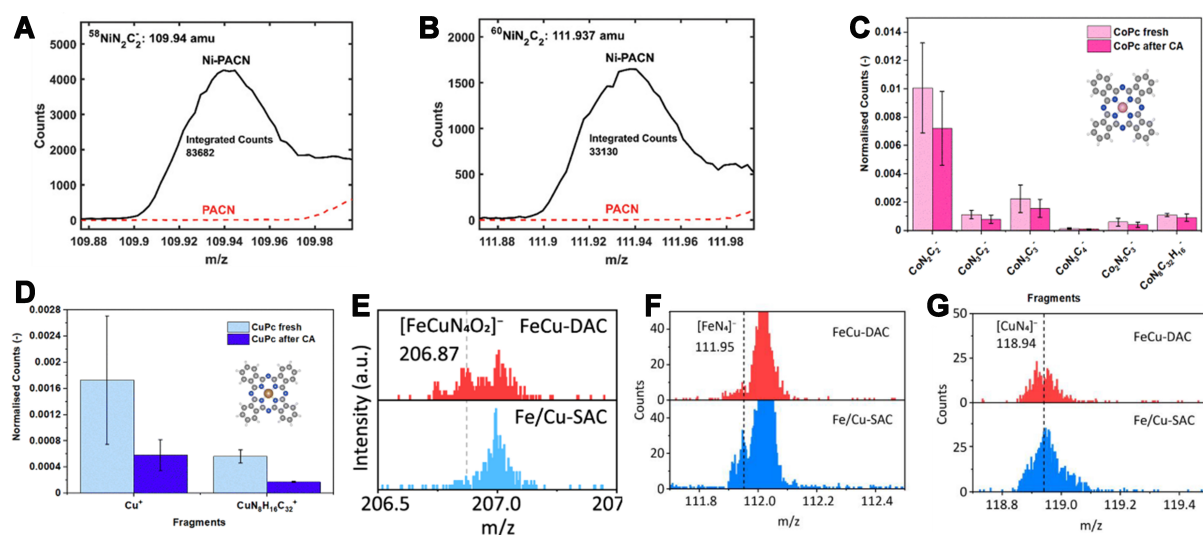


Figure 13. Comparison of ToF-SIMS intensity of NiPACN-3.5 wt% and metal-free PACN: (A) at $m/z = 109.94$ ($^{58}\text{NiN}_2\text{C}_2$ weight); (B) at $m/z = 111.94$ ($^{60}\text{NiN}_2\text{C}_2$ weight)^[10]. Copyright 2020, Wiley-VCH; ToF-SIMS positive spectrum results of (C) CoPc and (D) CuPc before and after constant potential measurements^[11]. Copyright 2023, The Royal Society of Chemistry; The ToF-SIMS spectra of FeCu-DAC and Fe/Cu-SAC. Ionized fragments of (E) $[\text{FeCuN}_4\text{O}_2]^-$, (F) $[\text{FeN}_4]^-$, and (G) $[\text{CuN}_4]^-$ are compared for FeCu-DAC and Fe/Cu-SAC^[78]. Copyright 2023, American Chemical Society. ToF-SIMS: Time-of-flight secondary ion mass spectrometry; PACN: DAC: dual-atom catalyst; SAC: single-atom catalyst.

beam-ejected fragments^[78]. A reference Fe/Cu-SAC was prepared via ZIF-8 pyrolysis with co-impregnated Fe and Cu nitrates. The diatomic $[\text{FeCuN}_4\text{O}_2]^-$ fragment exhibits markedly higher intensity in FeCu-DAC than in Fe/Cu-SAC [Figure 13E], whereas the mononuclear $[\text{FeN}_4]^-$ and $[\text{CuN}_4]^-$ fragments display the opposite trend [Figure 13F and G]. This unambiguously demonstrates that FeCu-DAC preserves a $[\text{FeCuN}_4\text{O}_2]^-$ ensemble akin to its precursor, while Fe/Cu-SAC consists predominantly of discrete $[\text{FeN}_4]^-$ and $[\text{CuN}_4]^-$ motifs.

CONCLUSION AND OUTLOOK

SACs with asymmetric coordination structures have emerged as a frontier in energy-related electrocatalysis owing to their tunable electronic structures and distorted coordination geometries. Unlike conventional M-N_4 motifs, asymmetric SACs introduce heteroatom ligands, adjacent vacancies or multi-metal centers to break local symmetry, thereby modulating the d-band center, optimizing intermediate adsorption modes, and enabling *in-situ* structural reconfiguration during reaction. This often translates into markedly enhanced activities for ORR, OER, CO_2RR , and beyond.

Synthesis of asymmetric SACs predominantly employs spatial-confinement strategies. MOFs, defect-rich carbon, or organic ligands serve as templates to prearrange metal precursors into predefined asymmetric sites, which are then fixed by high-temperature pyrolysis. In MOF-based routes, for instance, bimetallic complexes are assembled via electrostatic adsorption, macrocyclic-ligand mediation, or pre-coordination, encapsulated within the MOF matrix, and converted into atomically dispersed dual-atom or multi-atom centers upon carbonization. While monometallic or isolated bimetallic constructs are now well established, fabrication of heteronuclear multi-metal asymmetric sites remains challenging, necessitating precise precursor design to minimize random aggregation.

Asymmetric coordination imposes electronic perturbations that shift metal d-band centers more negatively relative to symmetric analogs, weakening undesired overbinding of oxygenated intermediates and reshaping the free-energy landscape. In multi-metal DACs, synergistic interactions between neighboring metal sites enable tandem catalysis: one site activates an intermediate while the other facilitates its conversion or desorption, thereby accelerating turnover and improving selectivity. Dynamic adaptation of active-site geometry - driven by *in situ* bond reorganization - further breaks linear scaling relations, unlocking higher intrinsic activities and customized product distributions.

Atomically precise SACs demand equally precise analytical tools. Aberration-corrected STEM coupled with EELS and XAS remains the workhorse for confirming SA dispersion, coordination numbers, and oxidation states. However, distinguishing subtle differences in geometric configuration, heteroatom identity, and mixed-metal composition in multi-metal SACs exceeds the capability of current techniques. Emerging methods - three-dimensional TEM/STEM tomography, *in-situ* scanning tunneling microscopy (STM), temporal analysis of products (TAP), and operando spectroscopies - are poised to reveal spatial heterogeneities, dynamic structural evolution, and reaction-specific active-site transformations with unprecedented resolution.

Although asymmetrically coordinated SACs have made considerable progress, they still face many challenges. (1) Precise synthesis of catalysts: High-temperature pyrolysis inherently introduces randomness, especially for heteronuclear multi-metal sites. Novel low-temperature or stepwise assembly protocols, guided by molecular-level precursors, are required to achieve uniform site construction; (2) Diversity and Scalability of catalysts: Extending beyond noble and late-transition metals to main-group and rare-earth elements could enrich the repertoire of asymmetric motifs. Moreover, scalable synthesis at gram to kilogram scale must be developed to meet industrial demands; (3) Stability of the catalyst: Unbalanced coordination numbers and heteroatom substitution can destabilize SACs under harsh ORR/OER conditions, leading to metal migration, aggregation, or carbon support corrosion. Engineering sinter-resistant supports and corrosion-resistant ligands is critical to preserve active-site integrity over prolonged cycles; (4) Selective Pathway Control: Although asymmetric sites tune adsorption energies, ensuring a single desired reaction pathway (e.g., four-electron ORR vs. two-electron H₂O₂ generation; CO₂ - CO vs. formate vs. hydrocarbons) remains a grand challenge. Rational design - combining DFT predictions with operando validation - is needed to suppress side reactions and enhance selectivity; (5) Mechanistic insights into catalysts: Current kinetic models often oversimplify cooperative multi-metal interactions and ignore dynamic site restructuring. Integrating *in situ* operando characterization with advanced theoretical frameworks will be indispensable for understanding reaction mechanisms and guiding targeted catalyst optimization.

DECLARATIONS

Authors' contributions

Conceived the project: Wan, J.; Wang, D.; Yu, R.

Wrote and edited the manuscript: Xia, T.; Wang, X.; Wan, J.; Qi, J.; Wang, D.; Yu, R.

All authors reviewed and approved the final version.

Availability of data and materials

Not applicable.

Financial support and sponsorship

This work was supported by the National Key Research and Development Program of China (No. 2024YFA1509400), National Natural Science Foundation of China (Nos. 22293043, 51932001, 51872024), and IPE Project for Frontier Basic Research, China (No. QYJC-2023-08). This work was carried out using

the facilities at Huairou Interdisciplinary Research Center for Engineering Mesoscience, CAS-IPE.

Conflicts of interest

All authors declared that there are no conflicts of interest.

Ethical approval and consent to participate

Not applicable.

Consent for publication

Not applicable.

Copyright

© The Author(s) 2025.

REFERENCES

1. Wei, Y.; Chen, K.; Kang, J.; Chen, W.; Wang, X.; Zhang, X. Policy and management of carbon peaking and carbon neutrality: a literature review. *Engineering* **2022**, *14*, 52–63. DOI
2. Deng, D.; Wu, J.; Feng, Q.; et al. Highly reversible zinc-air batteries at -40 °C enabled by anion-mediated biomimetic fat. *Adv. Funct. Mater.* **2024**, *34*, 2308762. DOI
3. Zheng, H.; Deng, D.; Zheng, X.; et al. Highly reversible Zn-air batteries enabled by tuned valence electron and steric hindrance on atomic Fe-N₄-C sites. *Nano. Lett.* **2024**, *24*, 4672–81. DOI PubMed
4. Yang, Q.; Jiang, Y.; Zhuo, H.; Mitchell, E. M.; Yu, Q. Recent progress of metal single-atom catalysts for energy applications. *Nano. Energy*. **2023**, *111*, 108404. DOI
5. Lin, Z.; Huang, H.; Cheng, L.; et al. Tuning the p-orbital electron structure of s-block metal Ca enables a high-performance electrocatalyst for oxygen reduction. *Adv. Mater.* **2021**, *33*, e2107103. DOI PubMed
6. Li, R.; Rao, P.; Wu, D.; et al. Understanding the bifunctional trends of Fe-based binary single-atom catalysts. *Adv. Sci.* **2023**, *10*, e2301566. DOI PubMed PMC
7. Zhao, Z. H.; Huang, J. R.; Liao, P. Q.; Chen, X. M. Highly efficient electroreduction of CO₂ to ethanol via asymmetric C-C coupling by a metal-organic framework with heterodimetal dual sites. *J. Am. Chem. Soc.* **2023**, *145*, 26783–90. DOI PubMed
8. Jiang, Y.; Huang, L.; Chen, C.; Zheng, Y.; Qiao, S. Catalyst–electrolyte interface engineering propels progress in acidic CO₂ electroreduction. *Energy. Environ. Sci.* **2025**, *18*, 2025–49. DOI
9. Liu, T.; Xu, T.; Li, T.; Jing, Y. Selective CO₂ reduction over γ-graphyne supported single-atom catalysts: crucial role of strain regulation. *J. Am. Chem. Soc.* **2024**, *146*, 24133–40. DOI
10. Sun, B.; Li, Z.; Xiao, D.; et al. Unveiling pH-dependent adsorption strength of *CO₂ intermediate over high-density Sn single atom catalyst for acidic CO₂-to-HCOOH electroreduction. *Angew. Chem. Int. Ed. Engl.* **2024**, *63*, e202318874. DOI PubMed
11. Wang, Y.; Li, Q.; Wang, M.; et al. Pumping electrons from oxygen-bridged cobalt for low-charging-voltage Zn-air batteries. *Nano. Lett.* **2024**, *24*, 13653–61. DOI
12. Bai, Y.; Deng, D.; Wang, J.; et al. Inhibited passivation by bioinspired cell membrane Zn interface for Zn-air batteries with extended temperature adaptability. *Adv. Mater.* **2024**, *36*, e2411404. DOI PubMed
13. Wang, Y.; Wu, J.; Tang, S.; et al. Synergistic Fe-Se atom pairs as bifunctional oxygen electrocatalysts boost low-temperature rechargeable Zn-air battery. *Angew. Chem. Int. Ed. Engl.* **2023**, *62*, e202219191. DOI PubMed
14. Li, Y.; Li, Y.; Sun, H.; et al. Current status and perspectives of dual-atom catalysts towards sustainable energy utilization. *Nanomicro. Lett.* **2024**, *16*, 139. DOI PubMed PMC
15. Wang, Y.; Su, H.; He, Y.; et al. Advanced electrocatalysts with single-metal-atom active sites. *Chem. Rev.* **2020**, *120*, 12217–314. DOI
16. Li, Z.; Li, B.; Li, Q. Single-atom nano-islands (SANIs): a robust atomic-nano system for versatile heterogeneous catalysis applications. *Adv. Mater.* **2023**, *35*, e2211103. DOI PubMed
17. Lyu, F.; Zeng, S.; Jia, Z.; et al. Two-dimensional mineral hydrogel-derived single atoms-anchored heterostructures for ultrastable hydrogen evolution. *Nat. Commun.* **2022**, *13*, 6249. DOI PubMed PMC
18. Liu, H.; Liu, C.; Zong, X.; Wang, Y.; Hu, Z.; Zhang, Z. Role of the support effects in single-atom catalysts. *Chem. Asian. J.* **2023**, *18*, e202201161. DOI PubMed
19. Han, L.; Cheng, H.; Liu, W.; et al. A single-atom library for guided monometallic and concentration-complex multimetallic designs. *Nat. Mater.* **2022**, *21*, 681–8. DOI PubMed
20. Jiang, Z.; Liu, X.; Liu, X. Z.; et al. Interfacial assembly of binary atomic metal-N_x sites for high-performance energy devices. *Nat. Commun.* **2023**, *14*, 1822. DOI PubMed PMC
21. Shen, R.; Hao, L.; Ng, Y. H.; et al. Heterogeneous N-coordinated single-atom photocatalysts and electrocatalysts. *Chin. J. Catal.*

- 2022, 43, 2453-83. DOI
22. Wu, H.; Xu, X.; Wu, J.; et al. Atomic engineering modulates oxygen reduction of hollow carbon matrix confined single metal-nitrogen sites for zinc-air batteries. *Small* **2023**, 19, e2301327. DOI PubMed
23. Tian, H.; Song, A.; Zhang, P.; et al. High durability of Fe-N-C single-atom catalysts with carbon vacancies toward the oxygen reduction reaction in alkaline media. *Adv. Mater.* **2023**, 35, e2210714. DOI PubMed
24. Zhang, S.; Ao, X.; Huang, J.; et al. Isolated single-atom Ni-N₃ catalytic site in hollow porous carbon capsules for efficient lithium-sulfur batteries. *Nano. Lett.* **2021**, 21, 9691-8. DOI PubMed
25. Li, Y.; Li, J.; Huang, J.; et al. Boosting electroreduction kinetics of nitrogen to ammonia via tuning electron distribution of single-atomic iron sites. *Angew. Chem. Int. Ed. Engl.* **2021**, 60, 9078-85. DOI PubMed
26. Lyu, L.; Hu, X.; Lee, S.; et al. Oxygen reduction kinetics of Fe-N-C single atom catalysts boosted by pyridinic N vacancy for temperature-adaptive Zn-air batteries. *J. Am. Chem. Soc.* **2024**, 146, 4803-13. DOI PubMed
27. Lu, X.; Li, Y.; Yang, P.; et al. Atomically dispersed Fe-N-C catalyst with densely exposed Fe-N₄ active sites for enhanced oxygen reduction reaction. *Chem. Eng. J.* **2024**, 485, 149529. DOI
28. Yin, S.; Li, Y.; Yang, J.; et al. Unveiling low temperature assembly of dense Fe-N₄ active sites via hydrogenation in advanced oxygen reduction catalysts. *Angew. Chem. Int. Ed. Engl.* **2024**, 63, e202404766. DOI PubMed
29. Yu, Y.; Wang, Y.; Yang, F.; et al. Meso/microporous single-atom catalysts featuring curved Fe-N₄ sites boost the oxygen reduction reaction activity. *Angew. Chem. Int. Ed. Engl.* **2025**, 64, e202415691. DOI PubMed PMC
30. Qin, Y.; Ou, Z.; Guo, C.; et al. Phosphor-doping modulates the d-band center of Fe atoms in Fe-N₄ catalytic sites to boost the activity of oxygen reduction. *Appl. Catal. B. Environ. Energy.* **2025**, 360, 124553. DOI
31. Luo, X.; Wei, X.; Wang, H.; et al. Secondary-atom-doping enables robust Fe-N-C single-atom catalysts with enhanced oxygen reduction reaction. *Nanomicro. Lett.* **2020**, 12, 163. DOI PubMed PMC
32. Liu, D.; Barbar, A.; Najam, T.; et al. Single noble metal atoms doped 2D materials for catalysis. *Appl. Catal. B. Environ.* **2021**, 297, 120389. DOI
33. Fan, M.; Cui, J.; Wu, J.; Vajtai, R.; Sun, D.; Ajayan, P. M. Improving the catalytic activity of carbon-supported single atom catalysts by polynary metal or heteroatom doping. *Small* **2020**, 16, e1906782. DOI PubMed
34. Chai, Y.; Dai, H.; Duan, X.; et al. Elucidation of the mechanistic origin of spin-state-dependent P-doped Fe single-atom catalysts for the oxidation of organic pollutants through peroxymonosulfate activation. *Appl. Catal. B. Environ.* **2024**, 341, 123289. DOI
35. Li, Y.; Wei, Z.; Sun, Z.; Zhai, H.; Li, S.; Chen, W. Sulfur modified carbon-based single-atom catalysts for electrocatalytic reactions. *Small* **2024**, 20, e2401900. DOI PubMed
36. Li, Z.; Wu, R.; Xiao, S.; et al. Axial chlorine coordinated iron-nitrogen-carbon single-atom catalysts for efficient electrochemical CO₂ reduction. *Chem. Eng. J.* **2022**, 430, 132882. DOI
37. Xu, J.; Zhang, S.; Liu, H.; et al. Breaking local charge symmetry of iron single atoms for efficient electrocatalytic nitrate reduction to ammonia. *Angew. Chem. Int. Ed. Engl.* **2023**, 62, e202308044. DOI PubMed
38. Li, Y.; Hu, J.; Zou, Y.; et al. Catalytic activity enhancement by P and S co-doping of a single-atom Fe catalyst for peroxymonosulfate-based oxidation. *Chem. Eng. J.* **2023**, 453, 139890. DOI
39. Tang, F.; Zhang, G.; Wang, L.; Huang, J.; Liu, Y. Unsymmetrically N, S-coordinated single-atom cobalt with electron redistribution for catalytic hydrogenation of quinolines. *J. Catal.* **2022**, 414, 101-8. DOI
40. Sun, T.; Wu, Q.; Che, R.; et al. Alloyed Co-Mo nitride as high-performance electrocatalyst for oxygen reduction in acidic medium. *ACS. Catal.* **2015**, 5, 1857-62. DOI
41. Chen, C.; Chai, J.; Sun, M.; et al. An asymmetrically coordinated ZnCoFe hetero-trimetallic atom catalyst enhances the electrocatalytic oxygen reaction. *Energy. Environ. Sci.* **2024**, 17, 2298-308. DOI
42. Huang, S.; Lin, F.; Wang, S.; et al. Asymmetric microenvironment tailoring strategies of atomically dispersed dual-site catalysts for oxygen reduction and CO₂ reduction reactions. *Adv. Mater.* **2024**, 36, e2407974. DOI PubMed
43. Cai, L.; Liu, Y.; Gao, Y.; et al. Atomically asymmetrical Ir-O-Co sites enable efficient chloride-mediated ethylene electrooxidation in neutral seawater. *Angew. Chem. Int. Ed. Engl.* **2025**, 64, e202417092. DOI PubMed
44. Zhan, G.; Hu, L.; Li, H.; et al. Highly selective urea electrooxidation coupled with efficient hydrogen evolution. *Nat. Commun.* **2024**, 15, 5918. DOI PubMed PMC
45. Yang, X.; Song, W.; Liao, K.; et al. Cohesive energy discrepancy drives the fabrication of multimetallic atomically dispersed materials for hydrogen evolution reaction. *Nat. Commun.* **2024**, 15, 8216. DOI PubMed PMC
46. Wang, Y.; Yin, H.; Dong, F.; et al. N-coordinated Cu-Ni dual-single-atom catalyst for highly selective electrocatalytic reduction of nitrate to ammonia. *Small* **2023**, 19, e2207695. DOI PubMed
47. Zhou, Y.; Yang, W.; Utetiwbabo, W.; et al. Revealing of active sites and catalytic mechanism in N-coordinated Fe, Ni dual-doped carbon with superior acidic oxygen reduction than single-atom catalyst. *J. Phys. Chem. Lett.* **2020**, 11, 1404-10. DOI
48. Yu, D.; Ma, Y.; Hu, F.; et al. Dual-sites coordination engineering of single atom catalysts for flexible metal-air batteries. *Adv. Energy. Mater.* **2021**, 11, 2101242. DOI
49. Zhu, Z.; Yin, H.; Wang, Y.; et al. Coexisting single-atomic Fe and Ni sites on hierarchically ordered porous carbon as a highly efficient ORR electrocatalyst. *Adv. Mater.* **2020**, 32, e2004670. DOI PubMed
50. Li, R.; Wang, D. Superiority of dual-atom catalysts in electrocatalysis: one step further than single-atom catalysts. *Adv. Energy. Mater.* **2022**, 12, 2103564. DOI

51. Woldu, A. R.; Yohannes, A. G.; Huang, Z.; et al. Experimental and theoretical insights into single atoms, dual atoms, and sub-nanocluster catalysts for electrochemical CO₂ reduction (CO₂RR) to high-value products. *Adv. Mater.* **2024**, *36*, e2414169. DOI PubMed PMC
52. Zheng, X.; Liu, Y.; Yan, Y.; Li, X.; Yao, Y. Modulation effect in adjacent dual metal single atom catalysts for electrochemical nitrogen reduction reaction. *Chin. Chem. Lett.* **2022**, *33*, 1455-8. DOI
53. Chen, C.; Sun, M.; Zhang, F.; et al. Adjacent Fe site boosts electrocatalytic oxygen evolution at Co site in single-atom-catalyst through a dual-metal-site design. *Energy. Environ. Sci.* **2023**, *16*, 1685-96. DOI
54. Wan, J.; Zhao, Z.; Shang, H.; et al. In situ phosphatizing of triphenylphosphine encapsulated within metal-organic frameworks to design atomic Co₁-P₁N₃ interfacial structure for promoting catalytic performance. *J. Am. Chem. Soc.* **2020**, *142*, 8431-9. DOI PubMed
55. Li, Y.; Sun, H.; Ren, L.; et al. Asymmetric coordination regulating D-orbital spin-electron filling in single-atom iron catalyst for efficient oxygen reduction. *Angew. Chem. Int. Ed. Engl.* **2024**, *63*, e202405334. DOI PubMed
56. Li, X.; Yang, X.; Liu, L.; et al. Chemical vapor deposition for N/S-doped single Fe site catalysts for the oxygen reduction in direct methanol fuel cells. *ACS. Catal.* **2021**, *11*, 7450-9. DOI
57. Qu, Q.; Mao, Y.; Ji, S.; et al. Engineering the Lewis acidity of Fe single-atom sites via atomic-level tuning of spatial coordination configuration for enhanced oxygen reduction. *J. Am. Chem. Soc.* **2025**, *147*, 6914-24. DOI PubMed
58. Ren, S.; Wang, Y.; Shi, L.; et al. Transforming plastics to single atom catalysts for peroxymonosulfate activation: axial chloride coordination intensified electron transfer pathway. *Adv. Mater.* **2025**, *37*, e2415339. DOI PubMed
59. Yan, L.; Wang, C.; Wang, Y.; et al. Optimizing the binding of the *OOH intermediate via axially coordinated Co-N₅ motif for efficient electrocatalytic H₂O₂ production. *Appl. Catal. B. Environ.* **2023**, *338*, 123078. DOI
60. Liu, J.; Gong, Z.; Allen, C.; et al. Edge-hosted Fe-N₃ sites on a multiscale porous carbon framework combining high intrinsic activity with efficient mass transport for oxygen reduction. *Chem. Catal.* **2021**, *1*, 1291-307. DOI
61. Qin, Y.; Ou, Z.; Xu, C.; et al. Highly accessible single Mn-N₃ sites-enriched porous graphene structure via a confined thermal-erosion strategy for catalysis of oxygen reduction. *Chem. Eng. J.* **2022**, *440*, 135850. DOI
62. Zhang, T.; Han, X.; Liu, H.; et al. Quasi-double-star nickel and iron active sites for high-efficiency carbon dioxide electroreduction. *Energy. Environ. Sci.* **2021**, *14*, 4847-57. DOI
63. Han, A.; Wang, X.; Tang, K.; et al. An adjacent atomic platinum site enables single-atom iron with high oxygen reduction reaction performance. *Angew. Chem. Int. Ed. Engl.* **2021**, *60*, 19262-71. DOI PubMed
64. Zhao, L.; Cai, Q.; Mao, B.; et al. A universal approach to dual-metal-atom catalytic sites confined in carbon dots for various target reactions. *Proc. Natl. Acad. Sci. U. S. A.* **2023**, *120*, e2308828120. DOI PubMed PMC
65. Li, Z.; Ji, S.; Wang, C.; et al. Geometric and electronic engineering of atomically dispersed copper-cobalt diatomic sites for synergistic promotion of bifunctional oxygen electrocatalysis in zinc-air batteries. *Adv. Mater.* **2023**, *35*, e2300905. DOI PubMed
66. Wu, J. X.; Chen, W. X.; He, C. T.; et al. Atomically dispersed dual-metal sites showing unique reactivity and dynamism for electrocatalysis. *Nanomicro. Lett.* **2023**, *15*, 120. DOI PubMed PMC
67. Zhang, Q.; Liu, D.; Zhang, Y.; et al. Insight into coupled Ni-Co dual-metal atom catalysts for efficient synergistic electrochemical CO₂ reduction. *J. Energy. Chem.* **2023**, *87*, 509-17. DOI
68. Wang, X.; Zhang, N.; Guo, S.; et al. p-d Orbital hybridization induced by asymmetrical FeSn dual atom sites promotes the oxygen reduction reaction. *J. Am. Chem. Soc.* **2024**, *146*, 21357-66. DOI PubMed
69. Zhu, J.; Xiao, M.; Ren, D.; et al. Quasi-covalently coupled Ni-Cu atomic pair for synergistic electroreduction of CO₂. *J. Am. Chem. Soc.* **2022**, *144*, 9661-71. DOI PubMed
70. Pan, F.; Jin, T.; Yang, W.; et al. Theory-guided design of atomic Fe-Ni dual sites in N,P-co-doped C for boosting oxygen evolution reaction. *Chem. Catal.* **2021**, *1*, 734-45. DOI
71. Sun, Z.; Luo, X.; Shang, H.; Wang, Z.; Zhang, L.; Chen, W. Atomic printing strategy achieves precise anchoring of dual-copper atoms on C₂N structure for efficient CO₂ reduction to ethylene. *Angew. Chem. Int. Ed. Engl.* **2024**, *63*, e202405778. DOI PubMed
72. Zhang, L.; Zhang, N.; Shang, H.; et al. High-density asymmetric iron dual-atom sites for efficient and stable electrochemical water oxidation. *Nat. Commun.* **2024**, *15*, 9440. DOI PubMed PMC
73. Zhang, T.; Jiang, J.; Sun, W.; et al. Spatial configuration of Fe-Co dual-sites boosting catalytic intermediates coupling toward oxygen evolution reaction. *Proc. Natl. Acad. Sci. U. S. A.* **2024**, *121*, e2317247121. DOI PubMed PMC
74. Zhao, S.; Liu, M.; Qu, Z.; et al. Cascade synthesis of Fe-N₂-Fe dual-atom catalysts for superior oxygen catalysis. *Angew. Chem. Int. Ed. Engl.* **2024**, *63*, e202408914. DOI PubMed
75. Sun, Z.; Li, C.; Wei, Z.; et al. Sulfur-bridged asymmetric CuNi bimetallic atom sites for CO₂ reduction with high efficiency. *Adv. Mater.* **2024**, *36*, e2404665. DOI PubMed
76. Li, R.; Zhang, Z.; Liang, X.; et al. Polystyrene waste thermochemical hydrogenation to ethylbenzene by a N-bridged Co, Ni dual-atom catalyst. *J. Am. Chem. Soc.* **2023**, *145*, 16218-27. DOI PubMed
77. Wang, B.; Yang, X.; Xie, C.; et al. A general metal ion recognition strategy to mediate dual-atomic-site catalysts. *J. Am. Chem. Soc.* **2024**, *146*, 24945-55. DOI PubMed
78. Zhang, Y. X.; Zhang, S.; Huang, H.; et al. General synthesis of a diatomic catalyst library via a macrocyclic precursor-mediated approach. *J. Am. Chem. Soc.* **2023**, *145*, 4819-27. DOI PubMed
79. Zhao, Y.; Chen, H. C.; Ma, X.; et al. Vacancy defects inductive effect of asymmetrically coordinated single-atom Fe-N₃S₁ active sites

- for robust electrocatalytic oxygen reduction with high turnover frequency and mass activity. *Adv. Mater.* **2024**, *36*, e2308243. DOI PubMed
80. Guan, G.; Liu, Y.; Li, F.; et al. Atomic cobalt metal centers with asymmetric N/B-coordination for promoting oxygen reduction reaction. *Adv. Funct. Mater.* **2024**, *34*, 2408111. DOI
81. Yin, L.; Zhang, S.; Sun, M.; Wang, S.; Huang, B.; Du, Y. Heteroatom-driven coordination fields altering single cerium atom sites for efficient oxygen reduction reaction. *Adv. Mater.* **2023**, *35*, e2302485. DOI PubMed
82. Shao, X.; Gan, R.; Rao, Y.; et al. Main group SnN_4O single sites with optimized charge distribution for boosting the oxygen reduction reaction. *ACS. Nano.* **2024**, *18*, 14742-53. DOI PubMed
83. Lin, X.; Zhang, X.; Liu, D.; et al. Asymmetric atomic tin catalysts with tailored p-orbital electron structure for ultra-efficient oxygen reduction. *Adv. Energy. Mater.* **2024**, *14*, 2303740. DOI
84. Huang, M.; Deng, B.; Zhao, X.; et al. Template-sacrificing synthesis of well-defined asymmetrically coordinated single-atom catalysts for highly efficient CO_2 electrocatalytic reduction. *ACS. Nano.* **2022**, *16*, 2110-9. DOI PubMed
85. Jin, Z.; Jiao, D.; Dong, Y.; et al. Boosting electrocatalytic carbon dioxide reduction via self-relaxation of asymmetric coordination in Fe-based single atom catalyst. *Angew. Chem. Int. Ed. Engl.* **2024**, *63*, e202318246. DOI PubMed
86. Wang, Q.; Dai, M.; Li, H.; et al. Asymmetric coordination induces electron localization at Ca sites for robust CO_2 electroreduction to CO. *Adv. Mater.* **2023**, *35*, e2300695. DOI PubMed
87. Liu, K.; Sun, Z.; Chen, W.; Lang, X.; Gao, X.; Chen, P. Ultra-fast pulsed discharge preparation of coordinatively unsaturated asymmetric copper single-atom catalysts for CO_2 reduction. *Adv. Funct. Mater.* **2024**, *34*, 2312589. DOI
88. Zhou, S.; Wei, W.; Cai, X.; et al. Customizing highly asymmetrical coordination microenvironment into P-block metal single-atom sites to boost electrocatalytic CO_2 reduction. *Adv. Funct. Mater.* **2024**, *34*, 2311422. DOI
89. Li, J.; Chen, Y.; Yao, B.; et al. Cascade dual sites modulate local CO coverage and hydrogen-binding strength to boost CO_2 electroreduction to ethylene. *J. Am. Chem. Soc.* **2024**, *146*, 5693-701. DOI PubMed
90. Li, F.; Qin, H.; Zhang, H.; et al. Another role of CO-formation catalyst in acidic tandem CO_2 electroreduction: local pH modulator. *Joule* **2024**, *8*, 1772-89. DOI
91. Chen, J.; Wang, D.; Yang, X.; et al. Accelerated transfer and spillover of carbon monoxide through tandem catalysis for kinetics-boosted ethylene electrosynthesis. *Angew. Chem. Int. Ed. Engl.* **2023**, *62*, e202215406. DOI PubMed
92. Li, Y.; Luo, X.; Wei, Z.; et al. Precisely constructing charge-asymmetric dual-atom Fe sites supported on hollow porous carbon spheres for efficient oxygen reduction. *Energy. Environ. Sci.* **2024**, *17*, 4646-57. DOI
93. He, N.; Sun, Y.; Chen, X.; Wang, J.; Liang, G.; Mo, F. Design of S, N-codoped Co-Fe dual-atom sites for efficient alkaline oxygen reduction. *J. Mater. Chem. A.* **2024**, *12*, 10101-9. DOI
94. Li, L.; Zhu, J.; Kong, F.; et al. Tailoring atomic strain environment for high-performance acidic oxygen reduction by Fe-Ru dual atoms communicative effect. *Matter* **2024**, *7*, 1517-32. DOI
95. Li, M.; Han, G.; Tian, F.; et al. Spin-polarized PdCu- Fe_3O_4 in-plane heterostructures with tandem catalytic mechanism for oxygen reduction catalysis. *Adv. Mater.* **2024**, *36*, e2412004. DOI PubMed
96. Chen, C.; Sun, Z.; Qin, G.; et al. Asymmetrically coordinated Cu dual-atom-sites enables selective CO_2 electroreduction to ethanol. *Adv. Mater.* **2024**, *36*, e2409797. DOI PubMed
97. Xie, Y.; Chen, X.; Sun, K.; et al. Direct oxygen-oxygen cleavage through optimizing interatomic distances in dual single-atom electrocatalysts for efficient oxygen reduction reaction. *Angew. Chem. Int. Ed. Engl.* **2023**, *62*, e202301833. DOI PubMed
98. Gao, Z.; Li, A.; Ma, D.; Zhou, W. Electron energy loss spectroscopy for single atom catalysis. *Top. Catal.* **2022**, *65*, 1609-19. DOI
99. Qi, H.; Yang, J.; Liu, F.; et al. Highly selective and robust single-atom catalyst Ru_1/NC for reductive amination of aldehydes/ketones. *Nat. Commun.* **2021**, *12*, 3295. DOI PubMed PMC
100. Qian, S.; Xu, F.; Fan, Y.; et al. Tailoring coordination environments of single-atom electrocatalysts for hydrogen evolution by topological heteroatom transfer. *Nat. Commun.* **2024**, *15*, 2774. DOI PubMed PMC
101. Roccapriore, K. M.; Torsi, R.; Robinson, J.; Kalinin, S.; Ziatdinov, M. Dynamic STEM-EELS for single-atom and defect measurement during electron beam transformations. *Sci. Adv.* **2024**, *10*, eadn5899. DOI PubMed PMC
102. Yang, J.; Liu, W.; Xu, M.; et al. Dynamic behavior of single-atom catalysts in electrocatalysis: identification of Cu- N_3 as an active site for the oxygen reduction reaction. *J. Am. Chem. Soc.* **2021**, *143*, 14530-9. DOI PubMed
103. Yang, Y.; Wang, Y.; Xiong, Y.; et al. In situ X-ray absorption spectroscopy of a synergistic Co-Mn oxide catalyst for the oxygen reduction reaction. *J. Am. Chem. Soc.* **2019**, *141*, 1463-6. DOI PubMed
104. Gorlin, Y.; Lassalle-Kaiser, B.; Benck, J. D.; et al. In situ X-ray absorption spectroscopy investigation of a bifunctional manganese oxide catalyst with high activity for electrochemical water oxidation and oxygen reduction. *J. Am. Chem. Soc.* **2013**, *135*, 8525-34. DOI PubMed PMC
105. Erickson, E. M.; Thorum, M. S.; Vasić, R.; et al. In situ electrochemical X-ray absorption spectroscopy of oxygen reduction electrocatalysis with high oxygen flux. *J. Am. Chem. Soc.* **2012**, *134*, 197-200. DOI PubMed
106. Zhu, Y.; Kuo, T.; Li, Y.; et al. Emerging dynamic structure of electrocatalysts unveiled by *in situ* X-ray diffraction/absorption spectroscopy. *Energy. Environ. Sci.* **2021**, *14*, 1928-58. DOI
107. Xu, Y. N.; Mei, B.; Xu, Q.; et al. In situ/operando synchrotron radiation analytical techniques for CO_2/CO reduction reaction: from atomic scales to mesoscales. *Angew. Chem. Int. Ed. Engl.* **2024**, *63*, e202404213. DOI PubMed
108. Pei, J.; Shang, H.; Mao, J.; et al. A replacement strategy for regulating local environment of single-atom $\text{Co-S}_x\text{N}_{4-x}$ catalysts to

- facilitate CO₂ electroreduction. *Nat. Commun.* **2024**, *15*, 416. DOI PubMed PMC
109. Weng, L. Advances in the surface characterization of heterogeneous catalysts using ToF-SIMS. *Appl. Catal. A. Gen.* **2014**, *474*, 203-10. DOI
110. Koshy, D. M.; Landers, A. T.; Cullen, D. A.; et al. Direct characterization of atomically dispersed catalysts: nitrogen-coordinated Ni sites in carbon-based materials for CO₂ electroreduction. *Adv. Energy. Mater.* **2020**, *10*, 2001836. DOI
111. Mukadam, Z.; Liu, S.; Pedersen, A.; et al. Furfural electrovalorisation using single-atom molecular catalysts. *Energy. Environ. Sci.* **2023**, *16*, 2934-44. DOI